



UNIVERSITÄT
BAYREUTH



Carbon and energy exchange at a submontane grassland site in an extremely dry year



Master thesis in geoecology

Valentin Heinzelmann

Student number: 1325878

supervised by

Dr. Wolfgang Babel

Prof. Dr. Christoph Thomas

Micrometeorology Group

University of Bayreuth

Bayreuth, July 2019

Contents

Abstract	1
Zusammenfassung	2
List of symbols and abbreviations	3
1. Introduction	4
2. Material and methods	9
2.1. Site description	9
2.2. Experimental setup	12
2.2.1. Data acquisition	13
2.2.2. Automatic weather station	13
2.2.3. Satellite data	13
2.3. Data analysis	14
2.3.1. Flux calculation	14
2.3.2. Quality control	15
2.4. Gap-filling and flux partitioning	18
2.4.1. Flux of carbon dioxide	18
2.4.2. Latent heat flux	18
2.5. Statistics	19
2.6. Indices	19
2.6.1. Water use efficiency	19
2.6.2. Light use efficiency	19
2.6.3. ET-ETpot and surface water balance	20
2.6.4. Standardized precipitation index	20
2.6.5. Q10-value	20
2.7. General conventions	21
3. Results	22
3.1. Climatic classification	22
3.2. Carbon fluxes	25
3.2.1. FORKAST 2010	25
3.2.2. GRACE 2018	25
3.3. Energy fluxes	28
3.3.1. Water fluxes	28
3.3.2. Water use efficiency	30
3.3.3. Bowen-ratio	30
3.3.4. Albedo	30

Contents

3.4. Carbon flux comparison	34
3.5. Environmental controls on carbon dioxide exchange	38
3.5.1. GPP in response to light and temperature	38
3.5.2. Ecosystem respiration in response to temperature and GPP	38
4. Discussion	40
4.1. Drought influence on ecosystem CO ₂ exchange	40
4.1.1. Gross primary production	41
4.1.2. Ecosystem respiration	41
4.1.3. Net ecosystem exchange	42
4.2. Drought influence on energy exchange	43
4.2.1. Energy fluxes	43
4.2.2. Water use efficiency	44
4.3. Uncertainty evaluation	45
4.3.1. Measurement uncertainty	45
4.3.2. Modelling uncertainty	46
4.3.3. Drought assessment	46
5. Conclusion	48
Bibliography	49
A. Appendix	56
A.1. GRACE 2018	56
A.1.1. Instruments	56
A.2. Forkast 2010	56
A.2.1. Parametrisation of net radiation	56
A.3. Photo series of the site	59
Declaration of Authorship	61

List of Figures

2.1.	Aerial image of the measurement site in Voitsumra, NE-Bavaria. The terrain is marked by slight shading. (Ref.: geoportal.bayern.de , state: 31.10.18, 14:03) . . .	10
2.2.	Aerial image of the close surrounding of the measurement site in Voitsumra. (Ref.: geoportal.bayern.de , state: 15.04.19, 16:45)	10
2.3.	Photo of the measurement site in Voitsumra taken towards North (17.10.18). . .	11
2.4.	Wind direction and velocity at the measurement site in Voitsumra in the second half of the year 2016.	11
2.5.	Close up photo of the eddy-covariance setup in Voitsumra taken towards west (04.10.18).	12
2.6.	Photo of the automatic weather station in Voitsumra towards North (24.07.18). .	14
2.7.	Nocturnal CO ₂ -flux F_c (30.07.18, 12:30 - 01.10.18 with quality criteria applied from Table 2.5) against friction velocity u_* . The solid vertical line marks the assessed u_* -threshold.	16
2.8.	Ensemble average CO ₂ -flux F_c for different wind sectors in the time period 31.07.18 - 15.10.18.	17
3.1.	Monthly mean temperature at Voitsumra for the climate period 1981-2010, the FORKAST 2010 reference year and GRACE 2018 (left). Yearly mean of the climate reference and yearly means for FORKAST and GRACE (right). Error bars indicate the standard deviations.	23
3.2.	Monthly precipitation sums at Voitsumra for the climate mean 1981-2010, the FORKAST 2010 reference year and GRACE 2018 (left). Yearly mean over the climate reference period and yearly sums for FORKAST 2010 and GRACE 2018 (right). Error bars indicate the standard deviations.	23
3.3.	Standardized Precipitation Index (SPI), based on six-month averages in the reference period 1981-2010 for the measurement site Voitsumra; the years 2010 and 2018 are marked by shaded areas. Blue and red points indicate extreme precipitation surplus and deficit, respectively.	24
3.4.	Cumulative net ecosystem exchange (NEE) for FORKAST 2010. Arrows mark mowing events, solid vertical lines confine the comparison period in the second growing season.	25
3.5.	Cumulative sums of the flux components gross primary production (GPP), net ecosystem exchange (NEE) and ecosystem respiration (R_{eco}) during FORKAST 2010.	26
3.6.	Cumulative net ecosystem exchange (NEE) during GRACE 2018; the solid vertical lines confine the comparison period.	26
3.7.	Cumulative sums of the flux components gross primary production (GPP), net ecosystem exchange (NEE) and ecosystem respiration (R_{eco}) during GRACE 2018.	27

List of Figures

3.8.	Net fluxes of carbon dioxide during GRACE 2018 displayed in a Hovmöller diagram. Solid lines show dawn and dusk, respectively.	27
3.9.	Cumulative surface water balance components and global radiation during GRACE 2018.	28
3.10.	Cumulative surface water balance components precipitation, evapotranspiration and the resulting balance in the comparison period during FORKAST 2010 and GRACE 2018.	29
3.11.	Global radiation and temperature in the comparison period during FORKAST 2010 and GRACE 2018.	29
3.12.	Comparison of bootstrapping-derived Q_e -means between FORKAST 2010 and GRACE 2018 in the comparison period. Arrows display the respective standard errors. The dashed line shows the 1:1 ratio, the solid line is the linear regression ($p < 0.001$).	30
3.13.	Drought indicator $ET \cdot ET_{pot}^{-1}$ during GRACE 2018. Filled circles mark days with mean daylight $ET_{pot} > 100 \text{ W m}^{-2}$	31
3.14.	$ET \cdot ET_{pot}^{-1}$ during FORKAST 2010 and GRACE 2018 in the comparison period. Filled circles show days with $ET_{pot} > 100 \text{ W m}^{-2}$	31
3.15.	Water use efficiency (WUE) during FORKAST 2010 and GRACE 2018 in the comparison period.	32
3.16.	Scatter plot of the mean daily Bowen-ratio during FORKAST 2010 and GRACE 2018 in the comparison period. The solid line displays the 1:1 ratio.	32
3.17.	Albedo at the measurement site during FORKAST 2010 and GRACE 2018. Filled circles show days with mean midday $K_{in} > 500 \text{ W m}^{-2}$	33
3.18.	Scatter plot between mean daily global radiation and mean daily temperature during FORKAST 2010 and GRACE 2018 in the comparison period.	33
3.19.	Comparison of cumulative net ecosystem exchange (NEE) based on daily sums between FORKAST 2010 and GRACE 2018 according to calendar date.	34
3.20.	Comparison of cumulative net ecosystem exchange (NEE) between FORKAST 2010 and GRACE 2018 in the comparison period.	35
3.21.	Comparison of the bootstrapping-derived mean net carbon fluxes between FORKAST 2010 and GRACE 2018 in the comparison period. Arrows display the respective standard errors. The dashed line shows the 1:1 ratio, the black line is the linear regression between the two years ($p < 0.001$).	36
3.22.	Cumulative flux components gross primary production (GPP) and ecosystem respiration (R_{eco}) during FORKAST 2010 and GRACE 2018 in the comparison period. Results are based on daily sums.	37
3.23.	Ratio between the cumulative sums of gross primary production (GPP) and ecosystem respiration (R_{eco}) for FORKAST 2010 and GRACE 2018 in the comparison period.	37
3.24.	Light use efficiency (LUE) of FORKAST 2010 and GRACE 2018 in the comparison period. Lines display the linear regressions for the respective years, both are significant ($p < 0.001$).	38
3.25.	Normalized difference vegetation index (NDVI) for the years 2010 and 2018.	39

List of Figures

3.26. Linear regressions of daily ecosystem respiration (R_{eco}) on mean daily air temperature for FORKAST 2010 and GRACE 2018 in the comparison period; both are significant ($p < 0.001$). Q10 values are based on exponential model (not shown).	39
A.1. Linear regression between calculated surface temperature and measured air temperature at 2m height in the time between 01.06.2010 - 01.09.2010. Solid line displays linear model.	57
A.2. Scatter plot between measured long-wave upwelling radiation ($I\uparrow$) (available data) and calculated $I\uparrow$ in the time period 01.06.2010 - 01.09.2010.	58
A.3. Series of photos of the measurement site taken during maintenance work.	60

List of Tables

2.1. Specifications of the eddy-covariance setup during FORKAST 2010 according to Haase (2010).	12
2.2. Specifications of the eddy-covariance setup during GRACE 2018.	13
2.3. List of the parameters measured by the automatic weather station during GRACE 2018.	13
2.4. Start and end time and date of the utilized data from FORKAST 2010 and GRACE 2018.	14
2.5. Applied plausibility ranges for further analysis of the GRACE 2018 and FORKAST 2010 data.	16
3.1. Cumulative fluxes of carbon, water and their relative deviation in the comparison period during FORKAST 2010 and GRACE 2018.	36
3.2. Mean daily carbon fluxes and their respective standard deviation in the comparison period during FORKAST 2010 and GRACE 2018.	36
A.1. Calibration values of the infrared-gas analyzer LiCor7500 S/N 0270.	56

Acknowledgement

Thanks to Prof. Dr. Christoph Thomas for the possibility of writing this work in the micrometeorology group and the positive working environment. Your feedback motivated and directed towards interesting new analyses. Furthermore, I want to thank Dr. Wolfgang Babel for the valuable support during all stages of the work. Beginning with the field set-up, continuing with data analysis and finally during the writing process, I always appreciated your straightforward help and feedback. For the technical assistance, I thank Johannes Olesch and Johann Schneider. Finally, I give my thanks to my friends and my family for encouragement and the nice time during my studies.

Abstract

Climate change causes higher frequencies of extreme climatic events like heat and drought which exert strong controls on ecosystem functioning. This study evaluates the impact of the extremely dry (-486 mm, thus 44% below average annual precipitation) and warm (2.1 °C above average annual temperature) year 2018 on the carbon (C) and energy dynamics of a submontane grassland site. In order to derive turbulent fluxes of carbon dioxide (CO_2), sensible and latent heat in a high temporal and spatial resolution, an eddy-covariance system has been set up in late summer. A comparison period in the second growing season, constrained by two mowing events, was defined. This facilitates a drought assessment in relation to the climatically normal year 2010. Gross primary production and ecosystem respiration were suppressed by 14% and 9% respectively. Mean daily net ecosystem exchange amounted to -1.2 g C m $^{-2}$ which corresponds to a reduction by 31%. It was further detected that the reaction to the main environmental drivers changed in response to drought. Light was used less efficiently during photosynthesis (comparison period 2010: 0.02 mol CO_2 (mol photons) $^{-1}$, 2018: 0.01 mol CO_2 (mol photons) $^{-1}$) and the temperature sensitivity of respiration decreased (Q10 2010: 1.89 and 2018: 1.56), which finally resulted in dampened C losses. Evapotranspiration was increased by 43% following a higher global radiation and an increased vapour pressure deficit. Nevertheless water limitation was obvious due to the surface water balance being in deficit over several days. This was supported by relating actual evapotranspiration to potential evapotranspiration ($ET \cdot ET_{pot}^{-1}$) which showed lower values than the reference. The higher energy input in the comparison period 2018 led to higher sensible heat fluxes, as reflected by increased Bowen ratios (2010: 0.26 (-), 2018: 0.45 (-)), approaching unity in some cases. The investigated site continued acting as a net C sink and showed a high regrowth potential, despite the pronounced drought. However, an increase in the frequency and intensity of extreme events, as expected within a changing climate, might further reduce net uptake and hence represent a positive feedback to climate change. Future management strategies should adapt to droughts by reducing the frequency of grass cuts.

Zusammenfassung

Im Zuge des Klimawandels steigt die Häufigkeit extremer klimatischer Ereignisse wie Hitzewellen und Dürren, die sich stark auf die Funktion von Ökosystemen auswirken. Die vorliegende Studie untersucht den Einfluss des extrem trockenen (-486 mm, damit 44% unterhalb des durchschnittlichen Jahresniederschlags) und warmen (2.1 °C über der Jahresmitteltemperatur) Jahres 2018 auf die Kohlenstoff (C)- und Energiebilanz eines submontanen Grünlands. Zur Bestimmung der turbulenten Flüsse an Kohlenstoffdioxid (CO_2), fühlbarer und latenter Wärme in hoher zeitlicher und räumlicher Auflösung wurde ein Eddy-Kovarianz System im Spätsommer aufgebaut. Es wurde eine Vergleichsperiode definiert, welche in der zweiten Wachstumsperiode zwischen zwei Mahden liegt. Dies ermöglicht, den Einfluss der Dürre im Verhältnis zu dem klimatisch normalen Jahr 2010 zu bewerten. Die Brutto-Primär-Produktion und Respiration waren um 14% beziehungsweise 9% reduziert. Der mittlere tägliche Netto-Ökosystem Austausch betrug -1.2 g C m⁻² d⁻¹, was einer Reduktion von 31% entspricht. Weiterhin wurde festgestellt, dass sich die Reaktion auf die wichtigsten Umweltfaktoren verändert hat. Licht wurde während der Photosynthese weniger effizient genutzt (in der Vergleichsperiode 2010: 0.02 mol CO_2 (mol photons)⁻¹, 2018: 0.01 mol CO_2 (mol photons)⁻¹) und die Temperaturempfindlichkeit der Respiration nahm ab (Q10 2010: 1.89 und 2018: 1.56), was letztendlich zu verringerten C-Verlusten führte. Die Evapotranspiration (ET) stieg um 43% als Folge der höheren Globalstrahlung und des gestiegenen Dampfdruckdefizits. Wasserlimitierung war dennoch ersichtlich aufgrund einer über mehrere Tage negativen Oberflächenwasserbilanz. Dies wurde bestätigt, indem die aktuelle ET zur potentiellen ET in Verhältnis gesetzt wurde, was verringerte Werte gegenüber der Referenz zeigte. Der höhere Energie-Eintrag während der Vergleichsperiode 2018 führte zu gestiegenen Flüssen an fühlbarer Wärme, wie anhand erhöhter Bowen-Verhältnisse (2010: 0.26 (-), 2018: 0.45 (-)) erkannt wurde, welche teilweise nahe 1 lagen. Der untersuchte Standort war trotz der ausgeprägten Dürre eine netto Senke für Kohlenstoff und zeigte ein hohes Nachwachs-Potential. Eine Zunahme extremer Ereignisse, wie es im Rahmen des Klimawandels erwartet wird, hat das Potential, die C-Aufnahme weiter zu reduzieren und stellt damit eine positive Rückkopplung zum Klimawandel dar. Strategien für ein zukünftiges Management sollten Dürren berücksichtigen, etwa durch eine Verringerung der Mahden.

List of symbols and abbreviations

Symbol	Description	Physical unit
AWS	Automatic weather station	-
C	Carbon	-
CO ₂	Carbon dioxide	-
EC	Eddy covariance	-
ET	Evapotranspiration	W m ⁻²
ET _{pot}	Potential evapotranspiration	W m ⁻²
F _c	Flux of carbon dioxide	μ mol m ⁻² s ⁻¹
FORCAST	Impact of climate change on ecosystems and climatic adaptation strategies	-
F _s	Storage flux of carbon dioxide	μ mol m ⁻² s ⁻¹
GPP	Gross primary production	μ mol m ⁻² s ⁻¹ / g C m ⁻²
GRACE	Grassland carbon and energy fluxes	-
I↓	Incoming long-wave radiation	W m ⁻²
I↑	Outcoming long-wave radiation	W m ⁻²
K↓	Incoming short-wave radiation	W m ⁻²
K↑	Outcoming short-wave radiation	W m ⁻²
LUE	Light use efficiency	mol CO ₂ (mol photons) ⁻¹
NDVI	Normalized difference vegetation index	-
NEE	Net ecosystem exchange	μ mol m ⁻² s ⁻¹ / g C m ⁻²
PAR	Photosynthetic active radiation	W m ⁻²
PPFD	Photosynthetic photon flux density	μ mol m ⁻² s ⁻¹
Q _e	Flux of latent heat	W m ⁻²
Q _h	Flux of sensible heat	W m ⁻²
Q _s [*]	Net radiation	W m ⁻²
R _{eco}	Ecosystem respiration	μ mol m ⁻² s ⁻¹ / g C m ⁻²
SPI	Standardized precipitation index	-
SWB	Surface water balance	mm
u _*	Friction velocity	m s ⁻¹
VPD	Vapour pressure deficit	hPa
WUE	Water use efficiency	g C (kgH ₂ O) ⁻¹

1. Introduction

The IPCC 2014 (Pachauri et al., 2014) describes a changing climate with rising temperatures and carbon dioxide (CO₂) as the main, anthropogenically enhanced greenhouse gas. Therefore, large effort went into a better scientific understanding of the global carbon (C) cycle. Its complexity is still only partly understood and nicely reflected by the term of a “boundless C cycle” (Battin et al., 2009), which was introduced to describe that also inland waters play a significant role in the C cycle. The inter-annual concentration variability of CO₂ is mainly caused by the terrestrial biosphere, therefore the capacity of CO₂ sinks is seen as a crucial part for the prediction of future CO₂-levels (Le Quéré et al., 2009).

Climate scenarios predict higher frequencies of drought and an increased precipitation variability for mid and high latitudes (Houghton et al., 2001; Pachauri et al., 2014). The intensively studied year 2003 with its extremely warm and dry summer has been found to even represent average conditions in climate simulations for 2070 - 2100 (Schär et al., 2004). Meanwhile, the impact of extreme weather events under rising CO₂ concentrations on the C balance of ecosystems is still not fully understood (Reichstein et al., 2013), underscoring the need of a deeper investigation.

Research has strongly focused on forest ecosystems, where initiatives for long-term measurement networks like FLUXNET led to an increased understanding of the C and water coupling in response to climatic conditions (Baldocchi et al., 2001). Compared to this, grassland studies are under-represented and the availability of long-term flux series has been limited (Wohlfahrt et al., 2008a).

Grasslands cover around 20% of Europe’s land surface (Berry et al., 2016) and are often managed, either grazed by livestock or seasonally mowed for the purpose of hay or silage production. They are counted as one of the most species-rich ecosystem types in Europe (Wilson et al., 2012), hence they are regarded as highly valuable from the perspective of nature conservation. Additionally, they provide important ecosystem services, for example by retaining deposited nitrogen surpluses (Phoenix et al., 2003) and therefore improve drinking water quality which might however not be the case for fertilized grasslands.

As for any ecosystem, grassland net ecosystem exchange (NEE) of CO₂ is ultimately regulated by gross primary production (GPP) in biomass accrual and outputs via ecosystem respiration (R_{eco}), which comprises autotrophic respiration by plant tissue (roots and shoots) and heterotrophic respiration by soil organisms. By subtracting harvest outputs, which are an important C flux in managed grasslands, net biome production is obtained (e.g. Soussana et al., 2007). Gilmanov et al. (2007) reviewed CO₂ flux measurements from 20 European grassland sites and reported annual NEE (i.e. neglecting harvest outputs) to range between strong sinks of $-650 \text{ g C m}^{-2} \text{ a}^{-1}$ and moderate sources of $160 \text{ g C m}^{-2} \text{ a}^{-1}$. For intensively managed grasslands of Atlantic climate, highest productivities were found, whereas extensively managed sites in southern Europe showed lower ones. Temperate and mountain grasslands in central Europe fell between the two extremes. Despite the wide range in the C balance, their role as a significant

C pool can be found as common agreement (Scurlock and Hall, 1998).

Management practices like mowing reduce productivity for a certain time period (e.g. Zeeman et al., 2010; Wohlfahrt et al., 2008b; Wolf et al., 2013; Riederer, 2014) and turn the ecosystem into a temporal C-source. However, management rather acts to increase productivity by keeping grasslands in a permanent stage of growth (Wohlfahrt et al., 2008b). Schmitt et al. (2010) found NEE and its underlying components to increase with management intensity. Interestingly, the ratio of $GPP \cdot R_{eco}^{-1}$ stayed approximately the same across the investigated sites, which demonstrates the tight coupling between those two flux components. The authors confirmed their findings by synthesizing flux measurements from grasslands around the globe.

Drought, as a disturbance of the water cycle, usually reduces NEE and its underlying components, which tends to turn ecosystems towards a net source of C to the atmosphere (van der Molen et al., 2011). In agreement with this, Ciais et al. (2005) reported substantial Europe-wide C losses during the severe summer heat and drought 2003. Compared to deep-rooting forests, grasslands have a small buffering capacity for soil water and are therefore prone to drought. On the other hand, they also show a high resilience to climate extremes and have a high potential for regrowth. Therefore, grasslands globally often prevail in dry regions (Reichstein et al., 2013).

Studies investigating drought impacts on C fluxes above grasslands mostly agree with regard to the observation that the flux components GPP and R_{eco} are reduced. However, differences are found for the reported net effects, hence the extent of the suppression of the components differs among the studies. For example, Hussain et al. (2011) and Jaksic et al. (2006) reported a slightly increased annual NEE, whereas mostly substantial decreases have been reported (Ammann et al., 2007; Nagy et al., 2007; Aires et al., 2008). Marcolla et al. (2011) found a grassland site to strongly adapt to changing environmental conditions, resulting in a dampened variability of annual C fluxes. All this highlights the necessity for a more detailed investigation of the included environmental drivers on the C cycling and their response to drought.

Turning to the energy exchange during heatwaves, which often occur together with droughts, grasslands show the important feature of increasing latent heat flux (Q_e) stronger than sensible heat flux (Q_h). Teuling et al. (2010) found that grasslands little regulated their stomata and thereby suppressed surface heating as long as soil moisture allowed. Contrary, forests reduced evapotranspiration (ET) by regulating their stomata and thereby increased the sensible heat flux. As soil drying proceeds at the grasslands, latent heat flux decreases and more energy is converted into sensible heat, representing a “critical shift” in the system. The exceptionally high temperatures during the summer heat 2003 are attributed to this mechanism by the authors. Hammerle et al. (2008) reported a significant influence of leaf area at a grassland site on its energy flux partitioning. Ground heat flux decreased, whereas albedo and ET increased with higher leaf area.

The coupling between C and water fluxes is described by the concept of water use efficiency (WUE) (e.g. Beer et al., 2009). It relies on the recognition that plants regulate their stomata in order to optimize the trade-off between C uptake and water loss. Adaptions of the ratio have been mainly observed for forests under drought conditions (e.g. Thomas et al., 2009) or under rising CO₂-concentrations (Keenan et al., 2013), but few studies report significant changes of the ratio for grasslands (e.g. Hussain et al., 2011), again indicating that stomata are less controlled in this ecosystem.

Precipitation and with this soil moisture is an important environmental driver for the C cycling in grasslands. The quantity mainly influences GPP (Chou et al., 2008), which is further

controlled by the amount of photosynthetic photon flux density (PPFD) representing the basis for photosynthesis. Evidently, the amount of assimilating plant matter itself also regulates GPP (Wohlfahrt et al., 2008a).

Light use efficiency (LUE) expresses the use of light in the photosynthetically active spectrum (400 - 700 nm) during GPP. It is among others used for a satellite-based, remote-sensing of GPP via multiplication of LUE by the absorbed photosynthetic active radiation (e.g. Turner et al., 2003). Moreover, it is applied to test for intra- and interannual variations in GPP, independent of the respective total radiative input. Thus, disturbances like grassland management (Gilmanov et al., 2007) or drought (Hussain et al., 2011; Aires et al., 2008) can be detected.

In turn, R_{eco} is mainly controlled by temperature (Lloyd and Taylor, 1994; Wohlfahrt et al., 2005a), assimilate supply (Bahn et al., 2008) and soil moisture. Dry conditions can cause substantial reductions and further reduce Q_{10} , the temperature sensitivity of respiration (e.g. Xu et al., 2004; Ruehr et al., 2010; Joos et al., 2010; Hussain et al., 2011). Drought influences all of the mentioned environmental drivers, most obviously, precipitation is reduced over a certain time period below the long-term average. In combination with above-average temperatures, also the vapour pressure deficit (VPD) increases, which potentially even enhances drought stress due to higher ET. Higher VPD might lead to decreased stomatal conductance, resulting in decreased C uptake.

An important puzzle to solve is how the flux components GPP and R_{eco} react to their main environmental drivers under drought stress. Reductions of GPP are expected to be more obvious due to water limitation, whereas R_{eco} might either dampen or enhance C losses. Eventually, this will help to explain the above-mentioned, partly opposed results reported for NEE sums under drought conditions. Moreover, understanding how drought impacts the C and energy coupling is essential for a better understanding of future climate scenarios.

The increasing impact of a changing climate on regional scales led to the research cooperation “FORCAST - Impact of climate change on ecosystems and climatic adaptation strategies” (2009 - 2012), initiated by the Bavarian Ministry of Science, Research and Art. One of its aims was to assess the impact of climatically extreme events on ecological processes and to elaborate possible adaptation strategies. Research covered different typical ecosystems found in Bavaria, among those, grasslands have been further investigated. In this context, Riederer et al. (2015) reviewed studies on C fluxes at eight European grassland sites which are in terms of the climatic conditions comparable to the investigated site in Voitsumra. Neglecting harvest outputs, a broad range in NEE from weak sources of $18 \text{ g C m}^{-2} \text{ a}^{-1}$ (Wohlfahrt et al., 2008b) to strong sinks of $-443 \text{ g C m}^{-2} \text{ a}^{-1}$ (Gilmanov et al., 2007) was observed. It turned out that Voitsumra with a budget of $-249 \text{ g C m}^{-2} \text{ a}^{-1}$ in 2010 falls well in the middle of the compared sites, which underscores its representativeness for extensively managed submontane grasslands.

In addition, the novel approach of combining a detailed process-level isotope-labelling experiment with the “top view” from the atmosphere, provided by the eddy-covariance (EC) method allowed to determine the absolute C input into individual ecosystem pools (Riederer et al., 2015). Drought plots with rainfall exclusion showed an increasing C allocation to below-ground pools. However, an assessment of the drought’s impact on the absolute C input was not possible (Riederer, 2014). This missing link led to the GRACE (**G**rassland **c**arbon and **e**nergy fluxes) experiment, since the exceptionally dry and warm conditions in 2018 provided the possibility for a natural, large-scale drought assessment.

Hence, the aim of this study is to explore the grassland’s C and energy dynamics during

a climatically extreme year in further detail, in order to gain insights into the ecosystem's reaction and the environmental controls on the fluxes. It is hypothesized that NEE of CO₂ is diminished compared to 2010, representing a reference year with average climatic conditions. Reduced NEE is expected to be mainly caused by lower GPP due to strong moisture limitations and thus less developed plant biomass. R_{eco} is expected to play a compensating role in the balance, since the temperature sensitivity is expected to be reduced under drought. Furthermore, the energy partitioning at the site is investigated representing an important topic with regard to climate feedbacks. In a broader context, the findings will help to understand how and whether extensively managed grassland sites are able to adapt to or even have the potential to mitigate expected climate extremes.

The eddy covariance method

For the determination of the NEE, the EC technique evolved as a well-established method (Baldocchi, 2003). Reynolds second postulate forms the basis for the EC-method:

$$\overline{xy} = \bar{x} \bar{y} + \overline{x'y'} \quad (1.1)$$

By using vertical wind speed w for variable x and CO₂-concentration c for y , eq. 1.1 simplifies to eq. 1.2, since mean wind speed $\bar{w} \equiv 0 \text{ m s}^{-1}$ when averaged over a sufficiently long period. Hence, the net flux F_c of CO₂ is expressed by (Foken, 2016) :

$$F_c = \overline{w'c'} = \frac{1}{N-1} \sum_{k=0}^{N-1} [(w_k - \bar{w})(c_k - \bar{c})] \quad (1.2)$$

Surface energy balance

The energy balance at the earth's surface is expressed as follows (Foken, 2016):

$$-Q_s^* = Q_h + Q_e + Q_g + \Delta Q_S \quad (1.3)$$

$-Q_s^*$ is net radiation, Q_h , Q_e and Q_g are the fluxes of sensible, latent and ground heat respectively (all in units of W m^{-2}). ΔQ_S is the storage term, generally describing the energy which is for example stored by plants. These components exert a strong control on ecological processes, since they influence soil and air temperatures. Further, Q_e determines among others the amount of plant-available water.

Potential evapotranspiration (ET_{pot}) describes a concept where Q_e is solely limited by energy input and water supply is infinite. Its calculation is derived from the recognition that the available energy is partitioned into the two turbulent fluxes Q_h and Q_e in the following way: $-Q_s^* + Q_g = Q_h + Q_e$ (assuming heat storage to be negligible). Building on it, Priestley and Taylor (1972) developed a formulation for the potential evapotranspiration:

$$ET_{pot} = \left(\alpha_{PT} \frac{-Q_s^* - Q_g}{\gamma \cdot s_c^{-1} + 1} \right) \quad (1.4)$$

α_{PT} is the Priestley-Taylor coefficient (1.25 (-)), γ is the psychrometric constant and s_c the slope of saturation vapour pressure curve. According to Foken (2016) their ratio can be approximated as: $\gamma \cdot s_c^{-1} = (-0.40 + 1.042 \cdot e^{0.0443 \cdot t})^{-1}$.

2. Material and methods

2.1. Site description

Measurements were taken at a submontane grassland site, located at 624 m a.s.l. (50°05′25″N, 11°51′25″E) at the edge of the Weißenstädter Becken in the Fichtelgebirge mountain range. The mountains “Großer Waldstein” (877 m a.s.l.) and “Schneeberg” (1051 m a.s.l.) are located north and south of the station, respectively (Riederer, 2014) (cf. fig 2.1) and thereby create a channelled wind flow at the open site in the west of the basin. Additionally, the site is subject to significant cold air pooling through its location in the valley and the hilly surroundings (Loos, 2016). This affects and complicates nighttime flux measurements, since turbulence intensity is usually suppressed under stably stratified conditions. Main prevailing wind direction is 250° WSW (see fig. 2.4); herefor, the year 2016 has been chosen since it contained little gaps, the second half of the year is shown, because the presented measurements are taken in the same time period. About 100 m south-east of the station, there is a small forest strip, c. 500 m north-west is the village Voitsumra (fig. 2.2). The surrounding is mainly composed of other managed grasslands and arable land (fig. 2.3).

The site has been extensively managed with mowing once or twice a year for a time period of more than 15 years without fertilization or slurry application. The soil type is Gleysol with a minimum thickness of 70 cm at the site. The plant community of the site is described as *Molinio-Arrhenatheretea*, Tx. 1937 economic grassland; dominant species are *Alchemilla monticola*, *Juncus filiformis*, *Polygonum bistorta*, *Ranunculus acris* and *Trifolium repens* (Riederer, 2014).

2.1. Site description

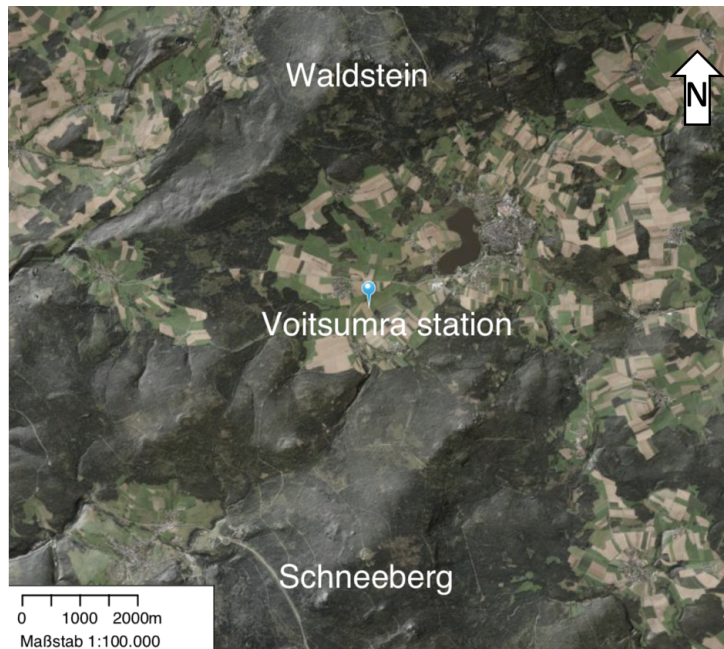


Figure 2.1.: Aerial image of the measurement site in Voitsumra, NE-Bavaria. The terrain is marked by slight shading. (Ref.: geoportal.bayern.de, state: 31.10.18, 14:03)

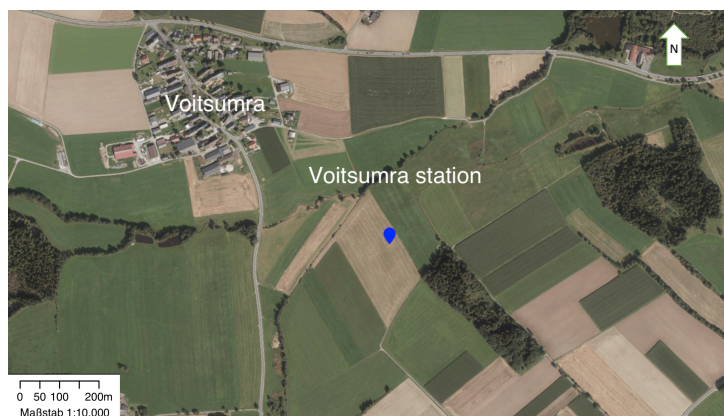


Figure 2.2.: Aerial image of the close surrounding of the measurement site in Voitsumra. (Ref.: geoportal.bayern.de, state: 15.04.19, 16:45)

2.1. Site description



Figure 2.3.: Photo of the measurement site in Voitsumra taken towards North (17.10.18).

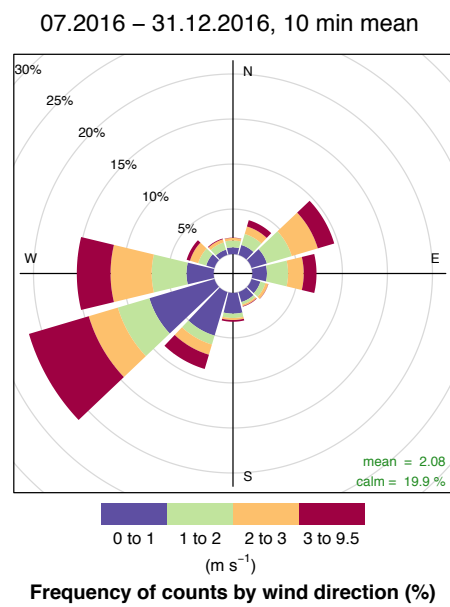


Figure 2.4.: Wind direction and velocity at the measurement site in Voitsumra in the second half of the year 2016.

2.2. Experimental setup

An EC system (see fig. 2.5), consisting of a 3D sonic anemometer (CSAT3, Campbell Scientific, Inc., Logan, Utah USA) has been set up on 30.07.2018. It points towards southeast in an azimuth angle of 150° , hence normal to the prevailing wind direction (cf. fig. 2.4). It was combined with an open-path gas analyzer (LI-7500, LI-COR Biosciences, Lincoln, Nebraska USA) for measurements of water vapor and CO_2 concentration, respectively (for calibration details refer to Table A.1). Refer to Table 2.2 for further details and an overview of the measured parameters.

Specifications of the EC system deployed during the FORKAST 2010-experiment (Haase, 2010) are shown in Table 2.1. Data from this field campaign will be used as a reference year.

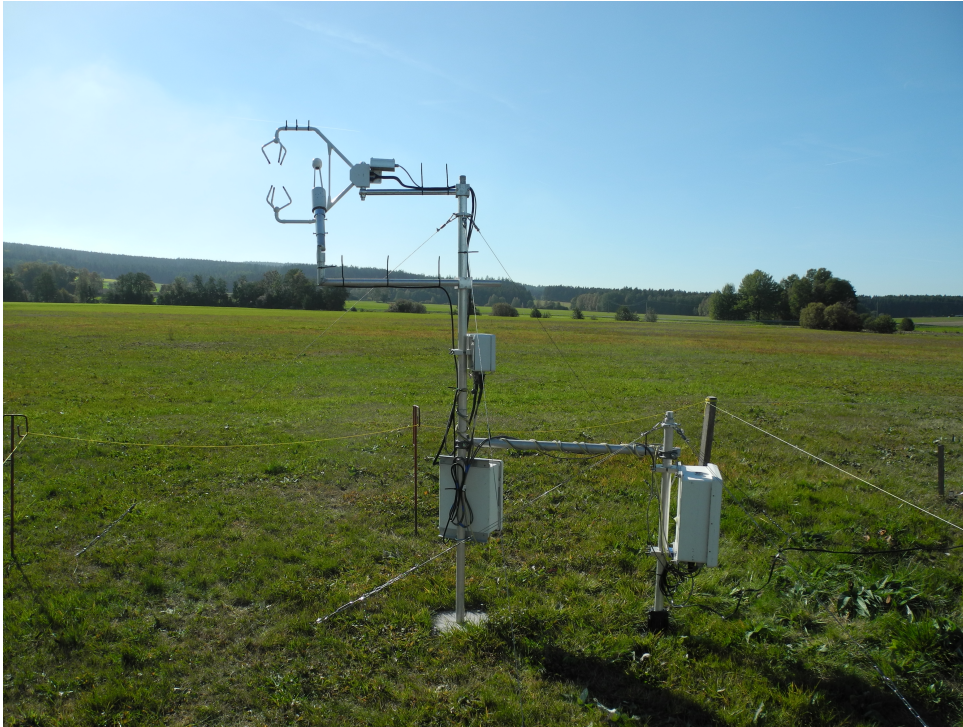


Figure 2.5.: Close up photo of the eddy-covariance setup in Voitsumra taken towards west (04.10.18).

Table 2.1.: Specifications of the eddy-covariance setup during FORKAST 2010 according to Haase (2010).

Device	S/N	Height of mean path length a.g.l. [m]	Azimuth angle
CSAT-3	0235	2.5	353°
LiCor-7500	75H-0220	2.4	5°

2.2. Experimental setup

Table 2.2.: Specifications of the eddy-covariance setup during GRACE 2018.

Device	S/N	Height of mean path length a.g.l. [m]	Azimuth angle	Parameter	Unit
CSAT-3	0205	2.02	150°	wind velocities u , v , w sonic temperature T_s	m s^{-1} °C
LiCor-7500	0270	2	155°	CO_2 - & H_2O - concentration	mmol m^{-3}

2.2.1. Data acquisition

The acquired data from the EC-system were recorded at 20 Hz frequency on a data logger (Model CR3000, Campbell Sci., Logan, UT, USA) of which the respective programme has been written by Dr. Wolfgang Babel (micrometeorology group, University of Bayreuth). Data have been collected on *CompactFlash* memory cards, which have been changed approximately biweekly.

2.2.2. Automatic weather station

10 min averages of the parameters (see Table 2.3) measured by the automatic weather station (AWS) in Voitsumra (fig. 2.6) were further used. Temperature and precipitation records have been mainly used for the climatic classification; the radiation measurements have been used for the gap-filling (F_c and Q_e) and for the calculation of ET_{pot} .

Table 2.3.: List of the parameters measured by the automatic weather station during GRACE 2018.

Device	Parameter	Unit
Pluvio	precipitation	mm
CNR4	$K \downarrow$, $K \uparrow$, $I \downarrow$, $I \uparrow$	W m^{-2}
HMP45	temperature, humidity	°C
Pt100	Soil temperature	°C
Cup anemometer	wind speed	m s^{-1}
Windvane	wind direction	°

2.2.3. Satellite data

The normalized difference vegetation index (NDVI), derived from MODIS (Moderate-resolution Imaging Spectroradiometer) instruments (on board of the satellites Aqua and Terra DAAC, 2018) was used to assess the condition of the plant biomass. It is based

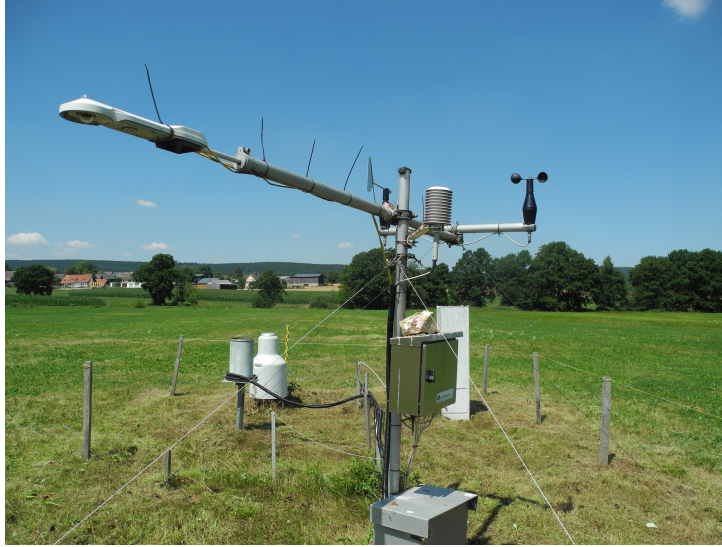


Figure 2.6.: Photo of the automatic weather station in Voitsumra towards North (24.07.18).

on a temporal resolution of 16 days and uses a spatial resolution of 250 m. Data with the product-intern usefulness description “lower quality” were excluded from the analysis, data flagged “decreasing quality” were included, in order to ensure sufficient data points.

2.3. Data analysis

The presented procedure has been used in the same way for data from FORKAST 2010 and GRACE 2018, in order to ensure comparability. Calendar start and end dates of the analysed experiments can be seen in Table 2.4.

Table 2.4.: Start and end time and date of the utilized data from FORKAST 2010 and GRACE 2018.

	FORKAST 2010	GRACE 2018
Start	01.01.2010, 00:30	30.07.2018, 12:30
End	20.12.2010, 23:30	13.12.2018, 16:00

Unless indicated differently, all data have been analysed by means of the *R* statistics software package (R Core Team, 2018) in combination with the editor *RStudio* (RStudio Team, 2016) (version 1.1.453). The packages “zoo” (Zeileis and Grothendieck, 2005) and “boot” (Canty and Ripley, 2017) have been used additionally.

2.3.1. Flux calculation

Acquired binary data were first transformed with the *CardConvert* tool from the *Logger-Net* programme (Campbell Sci., Logan, UT, USA) into the *TOA5*-format. Afterwards,

the *Camp2AsciiConverter*, a MATLAB programme written by Prof. Christoph Thomas (micrometeorology group, University of Bayreuth) was used for transforming the data into *csv*-format.

Subsequently, fluxes on a 30 min basis were calculated from the high-frequent 20 Hz data by means of the MATLAB programme *bmmflux* (version: 09.2017), developed by Prof. Christoph Thomas and described in Thomas et al. (2009).

The programme requires a user-defined configuration file, where among others plausibility ranges of $|u_{plausibility}| < 30 \text{ m s}^{-1}$ for the three wind components u , v and w were defined. For temperature values, the applied range was set to $-30 \text{ }^\circ\text{C} < T_{plausibility} < 50 \text{ }^\circ\text{C}$. Raw data not fulfilling the criteria are set to *NaN* by the programme. Spikes are removed from the data following the method of Vickers and Mahrt (1997).

Additionally, a frequency-response correction is performed (Moore, 1986). Fluxes are further corrected for density fluctuations (Webb et al., 1980) and buoyancy flux is converted into sensible heat flux by the SND-correction (Schotanus et al., 1983).

The file is divided into windows according to the perturbation time scale, which has been set to $T_p = 30 \text{ min}$. In these windows, measurements of the sonic anemometer are aligned to a new coordinate system, following a 3D rotation procedure. The first rotation takes place around the (vertical) z -axis, the second around the y -axis, so that $\bar{w} = 0$, which is essentially the prerequisite for eq. 1.2. Thirdly, the coordinate system is rotated such that it points into the mean wind direction with $\bar{v} = 0$. Finally, covariances and with this the fluxes of sensible and latent heat as well as CO_2 are calculated. The time interval used for the data in the presented thesis is shown in Table 2.4.

Subsequently, the storage flux (F_s) has been calculated, such that the net flux of CO_2 (F_c) consists of: $F_c = F_v + F_s$. F_s thereby describes the temporal change of the mean CO_2 -concentration within an air column extending from the ground up to the measurement height at 2.02 m, F_v is the vertical flux of CO_2 . Without advection, F_s vanishes; it has been approximated as:

$$F_{s,i} = \frac{\overline{\rho_{c,i}} - \overline{\rho_{c,(i-1)}}}{\Delta t} \cdot z_m \quad (2.1)$$

$\overline{\rho_{c,i}}$ denotes mean concentration of CO_2 (mmol m^{-3}) at time step i , Δt the time difference between step i and $i - 1$, in this case 30 min; z_m is the measurement height (m).

2.3.2. Quality control

Additionally, fluxes not fulfilling the following criteria were excluded from further data analysis:

1. Plausibility ranges for turbulent fluxes (values shown in Table 2.5).
2. Quality flags equal 2 (range: 0 - 2) are excluded. They follow the scheme achieved in the Spoleto agreement (2nd CarboEurope QA/QC workshop). The quality tests are in accordance to the procedure by Foken et al. (2004); see also Mauder and Foken (2015) for the conversion of the flags.

Table 2.5.: Applied plausibility ranges for further analysis of the GRACE 2018 and FORKAST 2010 data.

Parameter	Plausibility range	
F_c	-20 – 20	$\mu\text{mol m}^{-2} \text{s}^{-1}$
Q_e	-10 – 350	W m^{-2}
Q_h	-50 – 600	W m^{-2}
Quality flag	0, 1	-

In order to assure sufficient turbulent mixing, nighttime data below a visually assessed u_* -threshold of 0.15 m s^{-1} (fig. 2.7) had been excluded and therefore are replaced by modelled fluxes (see chapter 2.4). The issue arises from the measurement difficulty of when the true biological flux is measured and not because F_c and u_* have a causal dependency. Low turbulence conditions mostly come along with stable stratification, such that the biologically relevant signal might drain out of the control volume and not mix its way up to the sensor.

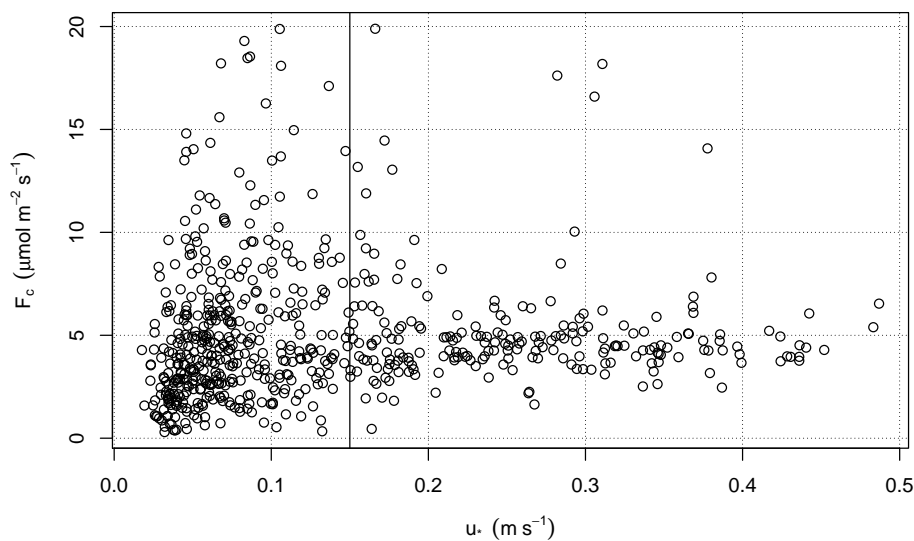


Figure 2.7.: Nocturnal CO_2 -flux F_c (30.07.18, 12:30 - 01.10.18 with quality criteria applied from Table 2.5) against friction velocity u_* . The solid vertical line marks the assessed u_* -threshold.

Footprint analysis

In context with the FORKAST project, Haase (2010) performed a Lagrangian footprint modelling according to Göckede et al. (2006). Even under stably stratified conditions, which tend to extend the footprint size, all measured data originated from grassland.

However the “Voitsumra” site, which is representative for the AWS (brighter surface in fig. 2.2) and the neighbouring site in the east (darker surface) were managed at the same time during FORKAST, hence no difference in the flux signal is expected.

During GRACE, however, management events differed. In order to pre check whether further data should be excluded, wind sector dependent ensemble average cycles were computed. The two selected sectors are based on the main wind sectors, occurring between 31.07.18 - 15.10.18, the time span being most relevant for C fluxes (see fig. 3.6). The cycles of F_c (fig. 2.8), Q_h and Q_e (latter ones not shown) did not differ significantly. Indeed, fig. 2.8 shows that “easterly” fluxes differed especially during nighttime from the westerly sector. However, the mean falls in the area confined by the standard deviations and it was presumed that replacing the measurements by modelled values would have further increased the uncertainty. Therefore, no data were excluded.

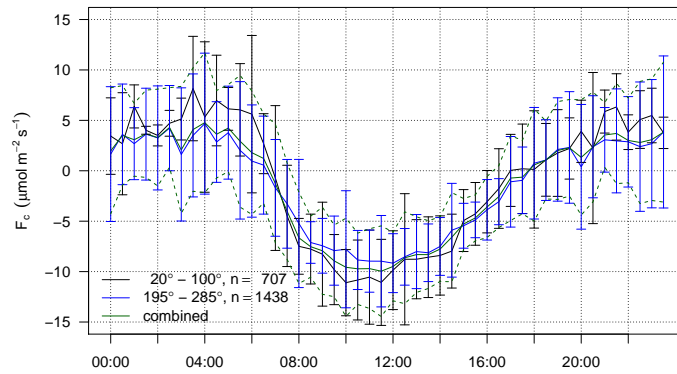


Figure 2.8.: Ensemble average CO_2 -flux F_c for different wind sectors in the time period 31.07.18 - 15.10.18.

2.4. Gap-filling and flux partitioning

The MATLAB programme *NEE-Tool-Terra*, developed by Prof. Christoph Thomas has been used for modelling the gaps in F_c , Q_e and to partition EC-derived net fluxes into their components GPP and R_{eco} .

2.4.1. Flux of carbon dioxide

Gaps in daytime NEE fluxes were calculated by a Michaelis-Menten type light-response model (Menten and Michaelis, 1913) for different temperature and radiation classes.

$$NEE = \frac{\alpha R_g F_{csat}}{\alpha R_g + F_{csat}} + R_{day} \quad (2.2)$$

With α being photon use efficiency (-), R_g is global radiation ($W m^{-2}$), F_{csat} saturation NEE flux ($\mu mol m^{-2} s^{-1}$) and R_{day} the daytime bulk respiration ($\mu mol m^{-2} s^{-1}$).

Nighttime fluxes, were used for parametrising R_{eco} with the Lloyd-Taylor temperature-response model (Lloyd and Taylor, 1994).

$$NEE = R_{10} e^{E_0 \left(\frac{1}{283.15 - T_0} - \frac{1}{T_{a,2m} + 273.15 - T_0} \right)} \quad (2.3)$$

R_{10} is the bulk respiration at a temperature of 10 °C, E_0 is a fit parameter (K), T_0 is the reference temperature set to 227.13 K and $T_{a,2m}$ is the air temperature (°C) at 2 m agl. Air temperature instead of soil temperature has been used for modelling, because of the results by Riederer et al. (2015), showing that around 2/3 of respiration takes place in the shoots and only 1/3 derives from soil efflux. By extrapolating nighttime NEE to daytime conditions, the partitioned flux component R_{eco} is obtained. In turn, gross uptake GPP is calculated as: $GPP = NEE - R_{eco}$ (see Ruppert et al., 2006, for the whole procedure).

Modelling led to spurious results of fluxes in temperature classes < 0 °C, hence assimilation (GPP) was set to 0 at these times and NEE was determined by R_{eco} . In the case of the FORKAST-data, the gap-filled fluxes behaved incorrectly during three days (21.08.10, 00:30 – 24.08.10, 00:00). Therefore, the components GPP, R_{eco} and NEE have been replaced by their respective ensemble average diurnal cycle of the preceding 37 days (15.07.10, 00:30 – 21.08.10, 00:00).

2.4.2. Latent heat flux

Gaps in latent heat fluxes Q_e are modelled by linearly regressing ET_{pot} against measured Q_e , calculated with the Priestley-Taylor method (Priestley and Taylor, 1972). Thereby, a constant ratio between Q_e and ET_{pot} is assumed.

$$ET = a \cdot ET_{pot} + b = a \left(\alpha_{PT} \frac{Q_s^* - 0.1|Q_s^*|}{\gamma \cdot s_c^{-1} + 1} \right) + b \quad (2.4)$$

The factors a and b represent the slope, respectively intercept of the linear model. The Priestley-Taylor method requires continuous values of net radiation ($-Q_s^*$), which in the case of FORKAST were partly parametrised as described in chapter A.2.1.

Remaining gaps (NA -values) in the F_c and Q_e time series due to missing temperature and radiation data were replaced by the following procedure:

1. Gaps of at maximum 5 hours in the 30-min fluxes were filled by linear interpolation.
2. Daily sums have been calculated, solely based on days without NA 's. Subsequently, NA 's contained in the time series of daily sum have been linearly interpolated from the neighbours.

2.5. Statistics

F_c and Q_e measurements (i.e. without gap-filling) of GRACE and FORKAST were directly compared to each other. In order to account for the differing number of data points, a bootstrapping approach has been used. It was performed within the programme R by resampling the available data in each radiation class 1,000 times with replacement. The calculation of the means is thereby based on different sub-samples. A bootstrapping-derived mean and standard error was then used for the analysis.

2.6. Indices

2.6.1. Water use efficiency

Daily sums of GPP and ET have been used for calculating WUE ($= GPP \cdot ET^{-1}$) (e.g. Beer et al., 2009).

Total measured ET encompasses bare soil evaporation, interception and transpiration, where only the latter one is linked to GPP. Therefore, rainfall days and the first two following days are commonly excluded from the analysis (Beer et al., 2009).

In order to ensure sufficient data in our analysis of the comparison period (see chapter 2.7) and to focus simultaneously on the transpiration part of ET, the following compromise has been decided for: days with rainfall sums exceeding 3 mm were excluded from the analysis, whereas post-rainfall days were left unchanged. Mean values indicated in the figures are derived by firstly calculating mean GPP and mean ET over the total comparison period. Then, the ratio has been calculated.

2.6.2. Light use efficiency

The photosynthetically active part (400 - 700 nm) has been estimated to be half of the total global radiation. Then, mean daily PPFD ($\mu\text{mol m}^{-2} \text{s}^{-1}$) has been calculated by using the widely applied conversion factor of 4.57 (e.g. McCree, 1972). This is of course a simplification, because no direct measurements of PAR are available at the site.

To assess the use of light in gross uptake, mean daily GPP ($\mu\text{ mol m}^{-2}\text{ s}^{-1}$) was linearly regressed on mean daily PPFD (comparable to Polley et al., 2011). Total incoming PAR is used and not exclusively its absorbed part, hence, the described procedure follows *ecological LUE* (Gilmanov et al., 2007). The respective LUE ($= GPP \cdot PPFD^{-1}$) is then reported as the mean over the comparison period. Equally to WUE, the values are calculated from the mean nominator and denominator, respectively.

2.6.3. ET-ET_{pot} and surface water balance

The ratio $ET \cdot ET_{pot}^{-1}$ is used in order to indicate drought stress via water fluxes. Solely ET -values from measured and approved data, hence no modelled fluxes were used. Similarly, based on the so derived, half-hourly ET time index, matching ET_{pot} values (calculated as shown in eq. 2.4) have been chosen. Then, daytime (i.e. half-hourly values with $K_{in} > 10\text{ W m}^{-2}$) means of each component and finally the respective ratios were calculated.

Surface water balance (SWB) is calculated as the difference between the cumulative values of precipitation and evapotranspiration. Negative values therefore indicate water deficit and positive ones water surplus. Water losses by surface runoff or infiltration are thereby not accounted for.

2.6.4. Standardized precipitation index

For the characterization of droughts on different temporal scales, the standardized precipitation index (SPI) is commonly used (McKee et al., 1993). It is calculated as follows:

$$SPI_i = \frac{P_i - P_{i,CP3}}{\sigma_{i,CP3}} \quad (2.5)$$

The mean precipitation $P_{i,CP3}$ and standard deviation $\sigma_{i,CP3}$ are derived for month i using a moving window of 6 months in climate period 3 (CP3: 1981 - 2010). Precipitation amount P_i in the same period of accumulation is then compared and normalized, which yields the index. Thereby, the position of each value can be indicated in the form of standard deviations from the mean. A moderate drought starts, when the standard deviation $\sigma < -1$.

2.6.5. Q10-value

R_{eco} was expressed by an exponential fit on air temperature (T_{air}) (procedure described by Hussain et al., 2011):

$$R_{eco} = a \cdot \exp(b \cdot T_{air}) \quad (2.6)$$

with a and b as fit parameters. b can be further expressed as: $b = \ln(Q_{10})/10$. Consequently, temperature sensitivity Q_{10} was calculated as:

$$Q_{10} = \exp(10b) \quad (2.7)$$

2.7. General conventions

Sign convention

The typical micrometeorological sign convention is used where negative signs indicate fluxes towards the surface and vice versa.

Reference year

The drought year 2018 will be compared to the reference year 2010, since the latter is closer to the long-term average precipitation conditions than 2018 (ref. to chap. 3.1).

Comparison period

In order to ensure comparability between the two experiments and to assess drought impacts, data were aligned according to the days after the first mowing instead to calendar dates. With this, the comparison is based on the second growing season of the respective years, defined by the management events. Under the same conditions, the site should be in the same stage of growth in both years and therefore show the same C dynamics. The overlap of the two datasets is constrained by the later measurement start of GRACE 2018 (Table 2.4), thus the comparison begins on day 29 instead of day 1 after mowing. The first and only mowing in 2018 was done on 01.07.18, therefore, day 29 after mowing corresponds to 31.07.18, one day after the measurement start. In the case of FORKAST 2010, day 29 is 06.08.10. The end of the comparison period is given by the second mowing during FORKAST 2010 on 23.09.10, day 77 after the first cut, hence a total of 48 days is compared.

The terms “GRACE” and “FORKAST” are used for the parts of the respective experiments which fall in the previously described comparison period. “FORKAST 2010” and “GRACE 2018” are used in order to refer to the total respective experimental period (see Table 2.4 for the dates). The captions deviate in order to simplify their understanding without reading through the text.

3. Results

3.1. Climatic classification

The year 2018 showed with 10.5 °C the highest mean annual air temperature ever recorded for Germany since 1881. Additionally, with only 586 mm precipitation, it is on place 4 of the driest years in the same time period, which made it even more exceptional (Friedrich and Kaspar, 2019).

Similar conditions were found for the measurement site in Voitsumra. With 7.6 °C mean annual temperature (fig. 3.1) and 627 mm (fig. 3.2) annual precipitation, it was the warmest, respectively driest year in the 1981 - 2010 reference period. The subset February - November was the driest period recorded since 1971 with 363 mm being distinctly below the mean of 892 mm for this subset in the 1981 - 2010 reference. Spring was initiated with an extraordinary temperature jump of the monthly mean temperature from -0.4 °C in March to 9.9 °C in April, being the warmest April since records began 1948.

The mean annual temperature in the reference year 2010 during the FORKAST experiment turned out to be distinctly below average, which was mainly due to the low autumn and especially winter temperatures. Contrary, summer temperatures were close to the climate mean.

Considering rainfall, the annual precipitation was with 1112 mm virtually equal to the mean of 1110 mm, which nearly doubled the amount of 2018. August stood out with its more than two times higher rainfall than the respective climate mean, which is important to note because the comparison period (see chapter 2.7) for the C fluxes lies within this interval. The remaining months were mostly within the range confined by the climatic standard deviation.

SPI in 2010 started with a mild drought (fig. 3.3), which was then relieved by high rainfalls in August (fig. 3.2). Contrary, 2018 had extremely dry conditions.

3.1. Climatic classification

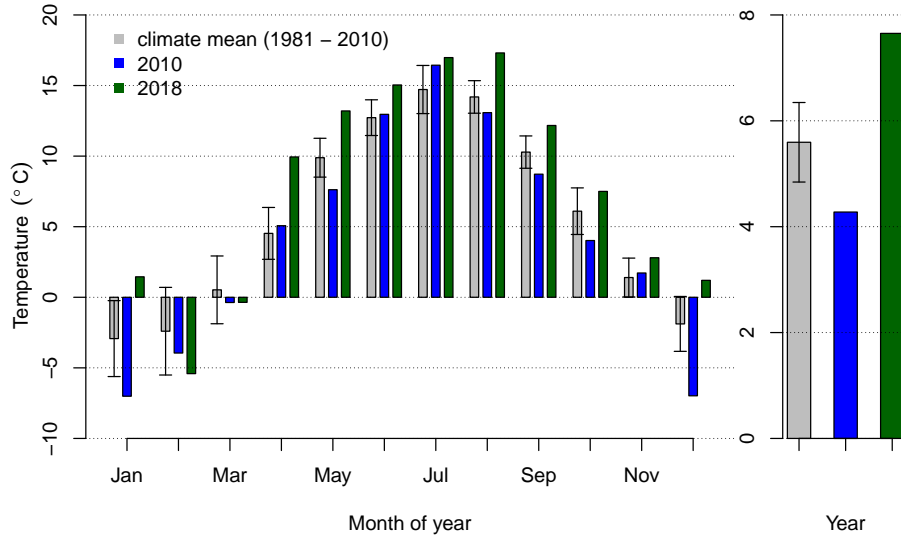


Figure 3.1.: Monthly mean temperature at Voitsumra for the climate period 1981-2010, the FORKAST 2010 reference year and GRACE 2018 (left). Yearly mean of the climate reference and yearly means for FORKAST and GRACE (right). Error bars indicate the standard deviations.

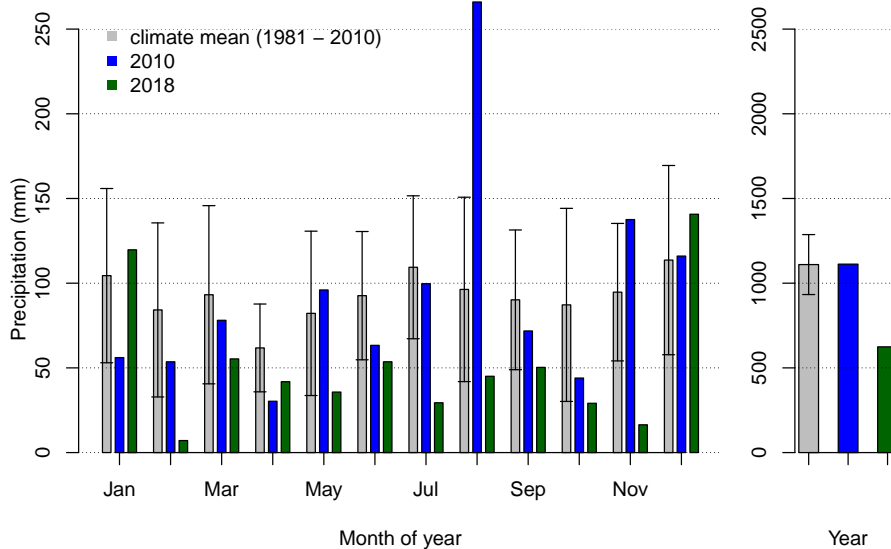


Figure 3.2.: Monthly precipitation sums at Voitsumra for the climate mean 1981-2010, the FORKAST 2010 reference year and GRACE 2018 (left). Yearly mean over the climate reference period and yearly sums for FORKAST 2010 and GRACE 2018 (right). Error bars indicate the standard deviations.

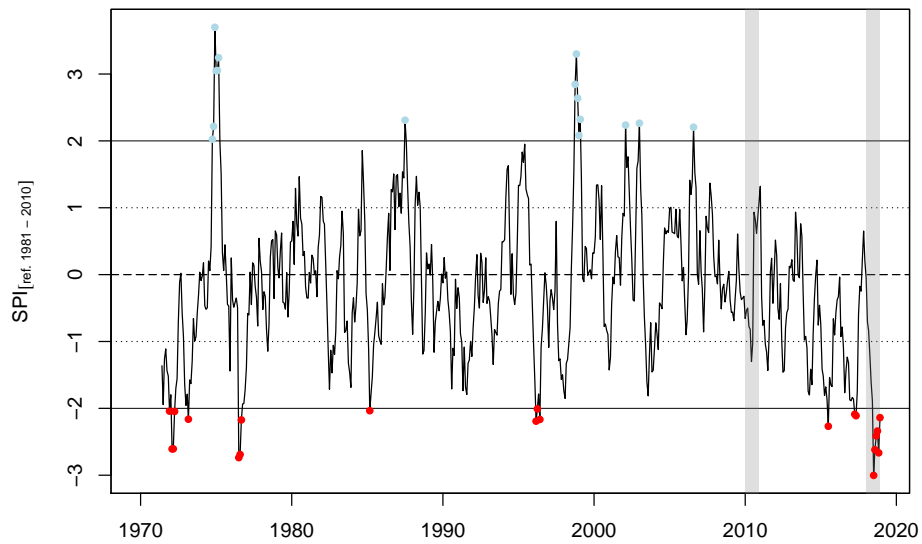


Figure 3.3.: Standardized Precipitation Index (SPI), based on six-month averages in the reference period 1981 - 2010 for the measurement site Voitsumra; the years 2010 and 2018 are marked by shaded areas. Blue and red points indicate extreme precipitation surplus and deficit, respectively.

3.2. Carbon fluxes

3.2.1. FORKAST 2010

The first mowing during FORKAST 2010 on 07.07.10 can be recognized in the cumulative sum of NEE, since it turned the site into a temporary C source (fig. 3.4). The second grass cut on 23.09.10 ended net uptake of C at the site for the year. The temporal subset 01.04.10 - 07.07.10, reflecting the window between onset of net C uptake and first mowing, showed highest mean daily NEE during FORKAST with $-2.9 \text{ g C m}^{-2} \text{ d}^{-1}$. Following the first mowing and neglecting its aftermath, the window 17.07.10 - 22.09.10 was chosen which yields with $-1.6 \text{ g C m}^{-2} \text{ d}^{-1}$ a lower mean daily NEE. The partitioned C fluxes are shown in fig. 3.5.

Data were available until 20.12.2010, therefore this day was taken as annual net sum amounting to -249 g C m^{-2} , which matches with the results from Riederer (2014). After addition of 158 g C m^{-2} harvest output (Riederer, 2014), -91 g C m^{-2} remained as net sum for 2010.

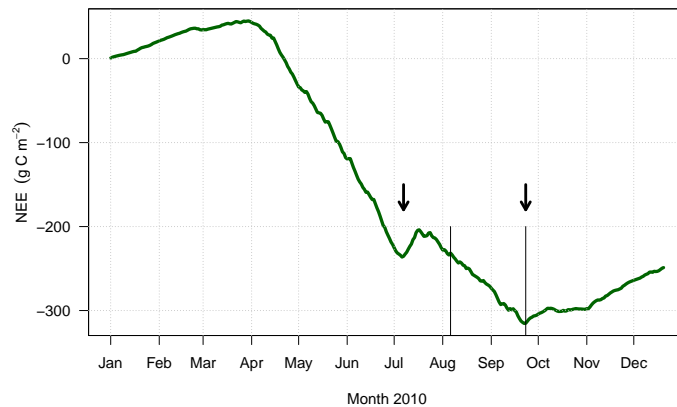


Figure 3.4.: Cumulative net ecosystem exchange (NEE) for FORKAST 2010. Arrows mark mowing events, solid vertical lines confine the comparison period in the second growing season.

3.2.2. GRACE 2018

The seasonal (see Table 2.4 for the dates) net uptake during GRACE amounted to -43 g C m^{-2} (fig. 3.6). The mean daily NEE in the time window with net C uptake from 31.07.18 - 21.10.18 amounted to $-1.1 \text{ g C m}^{-2} \text{ d}^{-1}$. Contrary to FORKAST, the site turned into a net C source without a second mowing. The respective flux components GPP and R_{eco} were both an order of magnitude larger than the resulting NEE (fig. 3.7).

Fig. 3.8 displays the daily and seasonal variability of the net C fluxes. High fluxes were observed even towards the end of the growing season. Therefore, they significantly contributed to the cumulative sum despite of the shorter daytime length.

3.2. Carbon fluxes

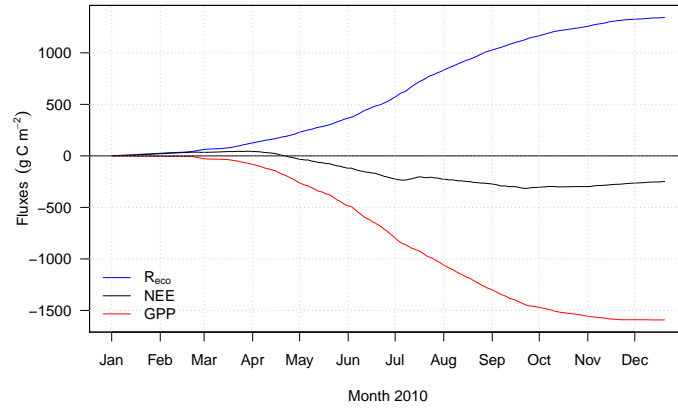


Figure 3.5.: Cumulative sums of the flux components gross primary production (GPP), net ecosystem exchange (NEE) and ecosystem respiration (R_{eco}) during FORKAST 2010.

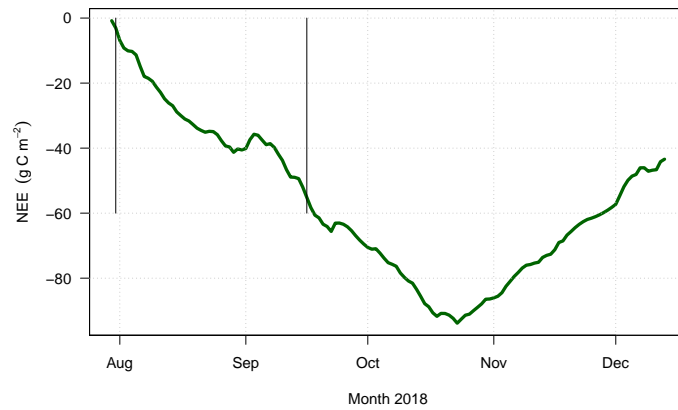


Figure 3.6.: Cumulative net ecosystem exchange (NEE) during GRACE 2018; the solid vertical lines confine the comparison period.

3.2. Carbon fluxes

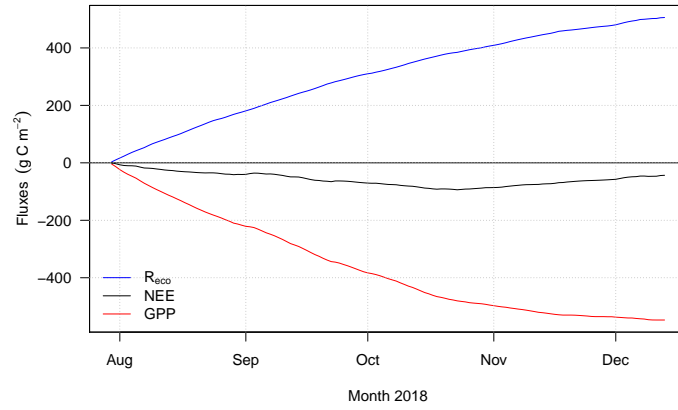


Figure 3.7.: Cumulative sums of the flux components gross primary production (GPP), net ecosystem exchange (NEE) and ecosystem respiration (R_{eco}) during GRACE 2018.

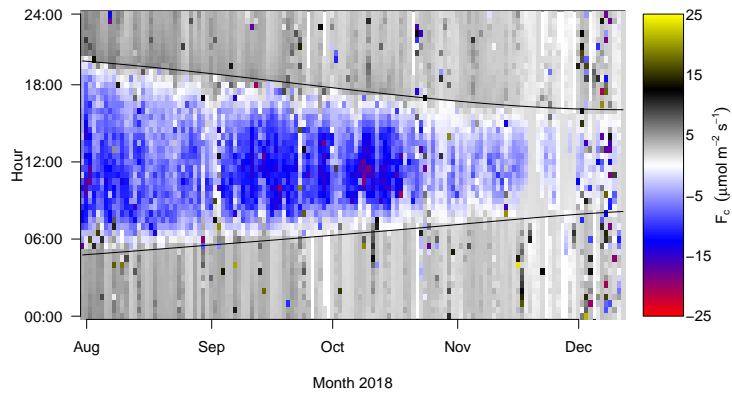


Figure 3.8.: Net fluxes of carbon dioxide during GRACE 2018 displayed in a Hovmöller diagram. Solid lines show dawn and dusk, respectively.

3.3. Energy fluxes

3.3.1. Water fluxes

The water balance during GRACE 2018 started with a slight deficit and then recovered to positive values due to lowered ET, which decreased concomitantly with global radiation (fig. 3.9).

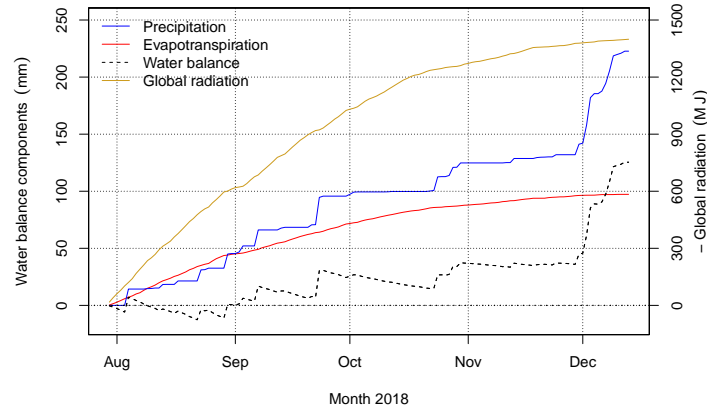


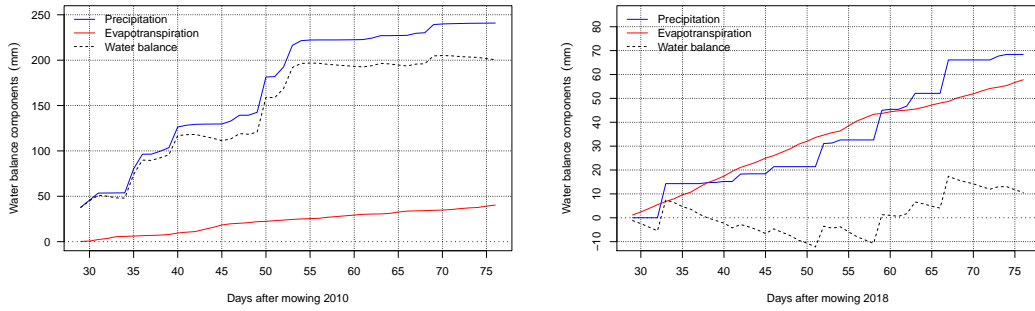
Figure 3.9.: Cumulative surface water balance components and global radiation during GRACE 2018.

The water balance components (fig. 3.10) in the comparison period of the two experiments differed distinctly. Precipitation in the investigated period prior to the second mowing amounted to 240.9 mm and 68.4 mm for FORKAST and GRACE, respectively. The SPI (fig. 3.3) during FORKAST equalled 0.9 and 0.8 in August and September and hence was close to normal conditions. Conversely, GRACE had values of -2.6 and -2.4 in the same months, indicating extreme precipitation deficits, also in the preceding months. FORKAST showed with 40.3 mm a lower ET than GRACE with 57.8 mm. Surface water balance ended up with a large surplus in 2010 (200.6 mm) and a small surplus in 2018 (10.6 mm).

These huge differences (fig. 3.10, Table 3.1) were not translated to higher ET during FORKAST. Instead, cumulative ET of GRACE exceeded FORKAST. The higher atmospheric demand was due to higher global and with this higher net radiation in 2018 (fig. 3.11). Additionally, mean daylight VPD, averaged over the comparison period, was with 11.4 hPa higher in 2018 than in 2010 (4.1 hPa). Noteworthy, the cumulative ET_{pot} during GRACE by far exceeded with 452 MJ m^{-2} the one from FORKAST with 278 MJ m^{-2} in the comparison period.

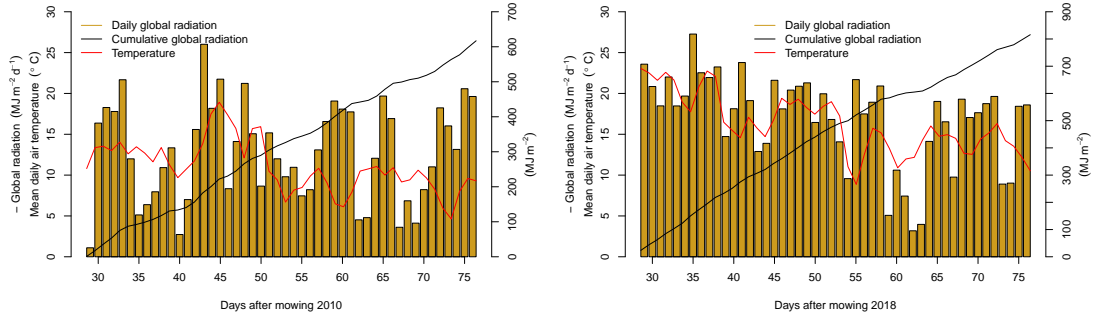
Grouping the water vapour fluxes of the comparison period in respective classes of global radiation and calculating the mean values using a bootstrapping approach, allowed to display them in a scatterplot, independent of the cumulative radiative input in the two years. It turned out, that ET per radiation class in the two years was nearly equal (fig. 3.12), suggesting that the observed rainfall deficits do not directly limit ET.

3.3. Energy fluxes



(a) Surface water balance components 2010. (b) Surface water balance components 2018.

Figure 3.10.: Cumulative surface water balance components precipitation, evapotranspiration and the resulting balance in the comparison period during FORKAST 2010 and GRACE 2018.



(a) Global radiation and temperature 2010. (b) Global radiation and temperature 2018.

Figure 3.11.: Global radiation and temperature in the comparison period during FORKAST 2010 and GRACE 2018.

The ratio of $ET \cdot ET_{pot}^{-1}$ was used as a measure of the proportion of ET_{pot} that can be reached by the available water. Thereby actual ET is water-limited whereas ET_{pot} is only limited by energy supply, reflected here as R_{net} (see eq. 2.4).

During GRACE 2018, the ratio (fig. 3.13) stayed at rather low values in August, then increased in response to a positive SWB, less energy input and thus lower ET_{pot} in September (fig. 3.9) and finally showed larger variation from mid October. This coincided with less energy input at the site, therefore mean daylight ET_{pot} fell below the threshold of 100 W m^{-2} . Thus, the site showed water limitation up to mid October and then shifted to energy limitation in the remaining measurement period.

Focusing on the comparison period, the ratio showed high scatter at higher values during FORKAST and consistently lower values with less variation during GRACE (fig. 3.14). This confirms the observed water limitation during GRACE, also found in the SWB (fig. 3.9).

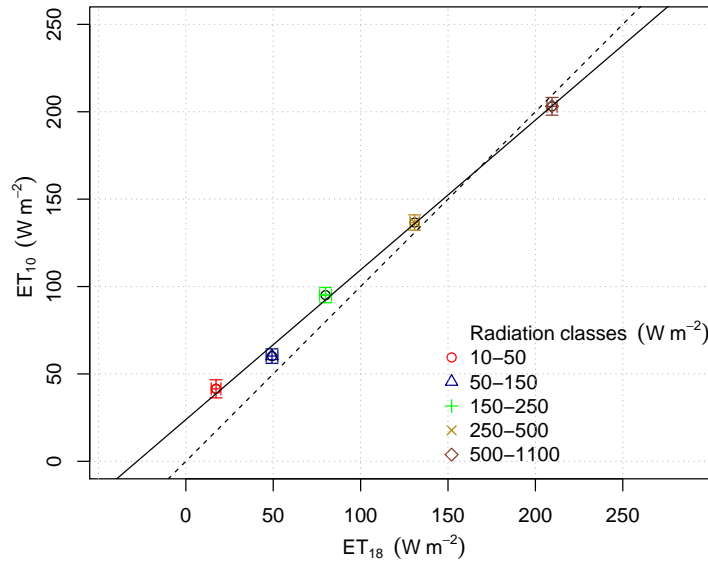


Figure 3.12.: Comparison of bootstrapping-derived Q_e -means between FORKAST 2010 and GRACE 2018 in the comparison period. Arrows display the respective standard errors. The dashed line shows the 1:1 ratio, the solid line is the linear regression ($p < 0.001$).

3.3.2. Water use efficiency

The carbon-water coupling was described as WUE. This measure turned out to be higher during FORKAST than during GRACE (fig. 3.15), caused by higher GPP (fig. 3.22a) concomitant with lower ET in this year (fig. 3.10a). Contrary, GRACE showed due to lower GPP (fig. 3.10b) and higher ET a reduced WUE.

3.3.3. Bowen-ratio

Mean Bowen-ratio during the comparison period during GRACE exceeded with 0.45 (–) the one during FORKAST with 0.26 (–) (fig. 3.16). This was despite the higher ET during GRACE (fig. 3.10b), hence the higher energy input (fig. 3.11b) lead to a proportionally stronger increase of Q_h than of ET.

3.3.4. Albedo

In 2018, the site has been mowed once on 01.07.2018 (personal communication by the farmer R. Purrucker). This can be seen in albedo changes (fig. 3.17b), where the first decrease was attributed to the grass cut of the surrounding grassland, the second mid July resulted from mowing at the AWS underneath the radiation sensor. During FORKAST 2010, the site has been mowed twice. First on 08.07.2010 and second on 23.09.2010.

Fig. 3.18 shows that mean daily temperatures during GRACE exceeded the ones from FORKAST in the comparison period at same values of daily global radiation.

3.3. Energy fluxes

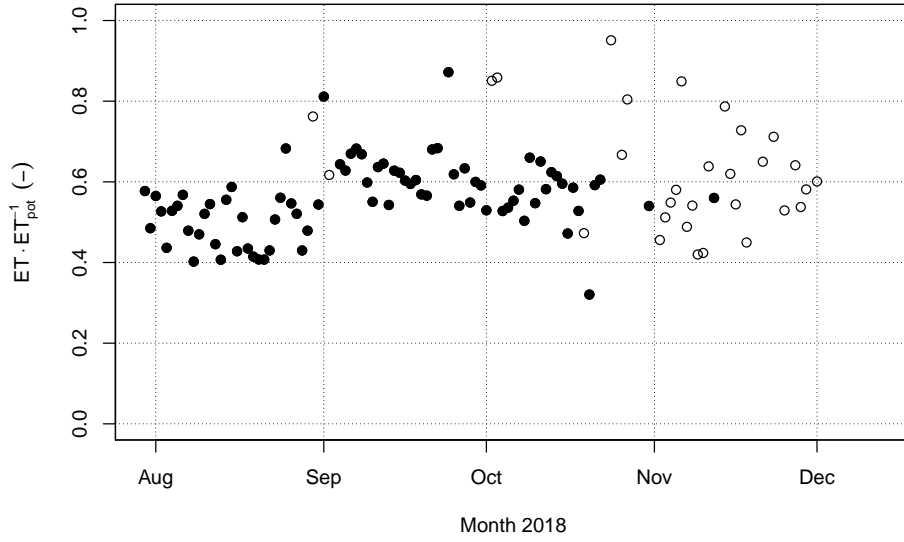
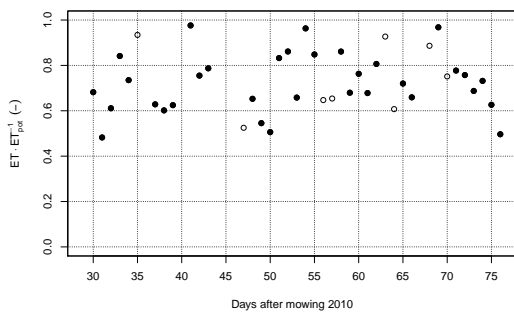
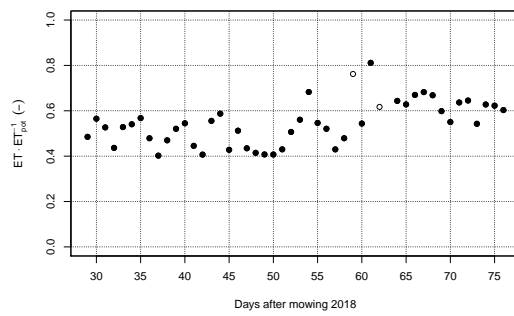


Figure 3.13.: Drought indicator $ET \cdot ET_{pot}^{-1}$ during GRACE 2018. Filled circles mark days with mean daylight $ET_{pot} > 100 \text{ W m}^{-2}$.



(a) $ET \cdot ET_{pot}^{-1}$ 2010.



(b) $ET \cdot ET_{pot}^{-1}$ 2018.

Figure 3.14.: $ET \cdot ET_{pot}^{-1}$ during FORKAST 2010 and GRACE 2018 in the comparison period. Filled circles show days with $ET_{pot} > 100 \text{ W m}^{-2}$.

3.3. Energy fluxes

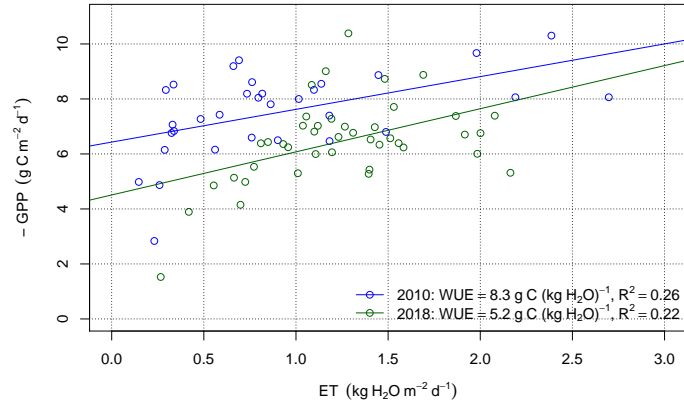


Figure 3.15.: Water use efficiency (WUE) during FORKAST 2010 and GRACE 2018 in the comparison period.

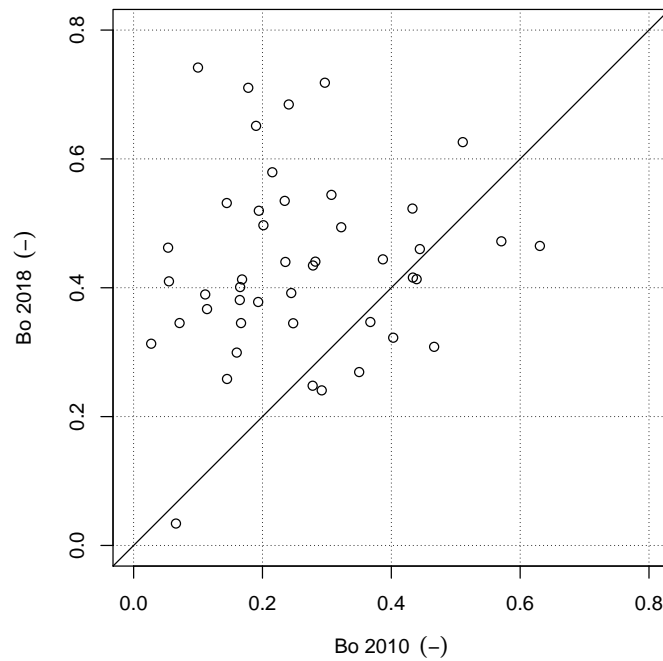
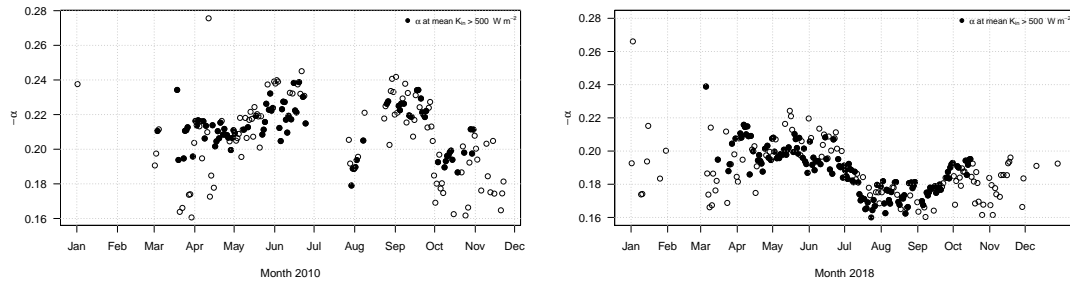


Figure 3.16.: Scatter plot of the mean daily Bowen-ratio during FORKAST 2010 and GRACE 2018 in the comparison period. The solid line displays the 1:1 ratio.

3.3. Energy fluxes



(a) Albedo in 2010.

(b) Albedo in 2018.

Figure 3.17.: Albedo at the measurement site during FORKAST 2010 and GRACE 2018. Filled circles show days with mean midday $K_{in} > 500 \text{ W m}^{-2}$.

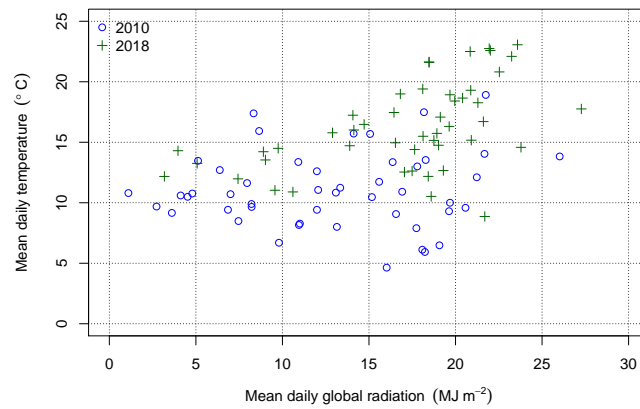


Figure 3.18.: Scatter plot between mean daily global radiation and mean daily temperature during FORKAST 2010 and GRACE 2018 in the comparison period.

3.4. Carbon flux comparison

Calendar dates

The comparison of the cumulative NEE sums between parts of FORKAST 2010 and the full experiment of GRACE 2018 based on calendar dates showed with -33.3 g C m^{-2} and -43.4 g C m^{-2} only a minor difference at the end (fig. 3.19). Most obvious is the interruption in net uptake due to the second mowing during FORKAST 2010 end of September, one month before GRACE turned into a net source.

In the case of FORKAST 2010, it can be further recognized that following the mowing-induced time period of being a C source, the site stayed at a net uptake of zero for nearly one month before it finally started continuously losing C.

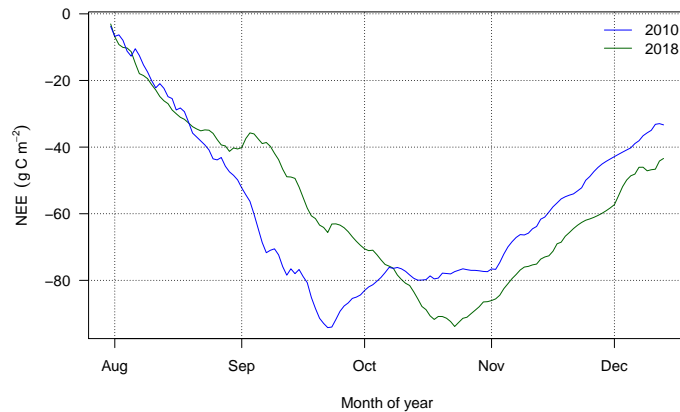


Figure 3.19.: Comparison of cumulative net ecosystem exchange (NEE) based on daily sums between FORKAST 2010 and GRACE 2018 according to calendar date.

Comparison period

Up to day 57 in fig. 3.20, both experiments showed about the same net uptake rate with slightly higher NEE during GRACE. From there on, the net uptake of GRACE slightly decreased, whereas FORKAST showed within 5 days a large net uptake of -17.4 g C m^{-2} . This difference was maintained and slightly increased until the end of the comparison, where FORKAST showed a -25.2 g C m^{-2} higher net uptake than GRACE (see Table 3.1). Correspondingly, mean daily fluxes were higher in the comparison period 2010 than in 2018 (Table 3.2), which resulted in 31% less net C uptake during GRACE compared to FORKAST.

Direct flux comparison

Apart from comparing the net sums, measured and approved fluxes falling in the comparison period were grouped in five classes of global radiation and compared to each other (fig. 3.21). This allowed to directly compare the two experiments without the confounding

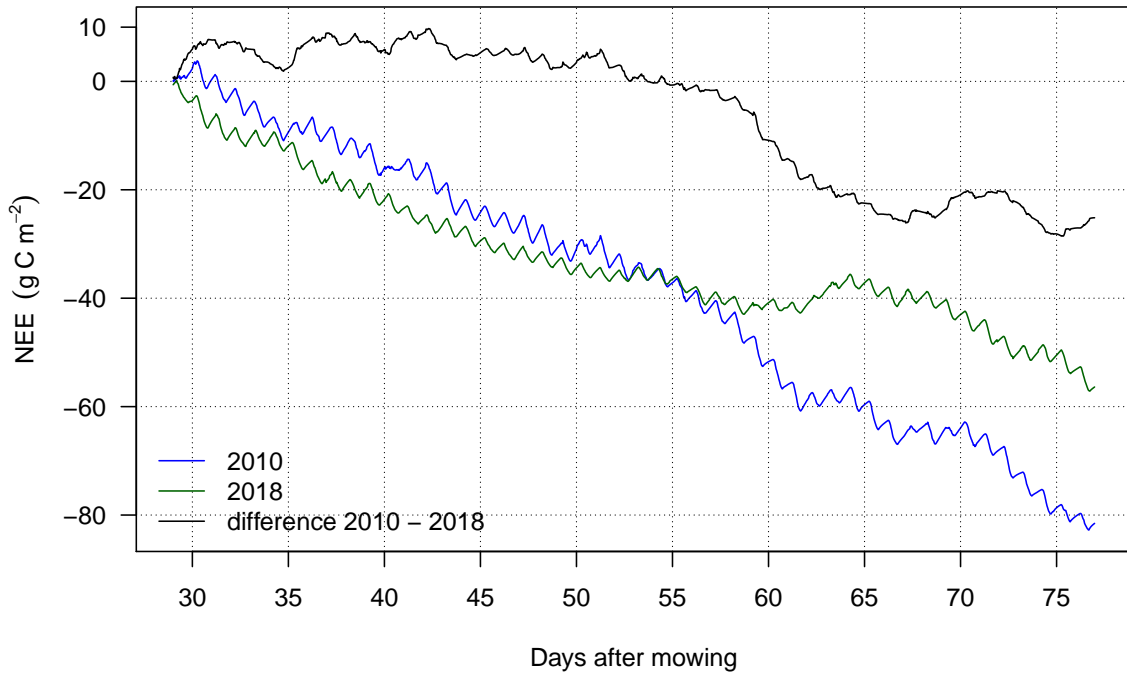


Figure 3.20.: Comparison of cumulative net ecosystem exchange (NEE) between FORKAST 2010 and GRACE 2018 in the comparison period.

effects of differing light regimes (fig. 3.11), being one of the major environmental drivers. It turned out that in the respective radiation classes, the net fluxes during FORKAST were significantly larger than during GRACE ($p < 0.001$). This implies that LUE for NEE is higher during FORKAST.

Flux components

The respective flux components GPP and R_{eco} for the two experiments behaved also differently (fig. 3.22). At the end of the comparison period GPP and R_{eco} differed by -49.2 g C m^{-2} and 23.9 g C m^{-2} , respectively. Higher GPP during FORKAST (fig. 3.22a) was not offset by its higher R_{eco} (fig. 3.22b), as displayed in the ratio between the components, which slightly increased with time (fig. 3.23). In the case of GRACE, however, the ratio decreased due to a stronger reduction of GPP than that of R_{eco} (Table 3.1).

3.4. Carbon flux comparison

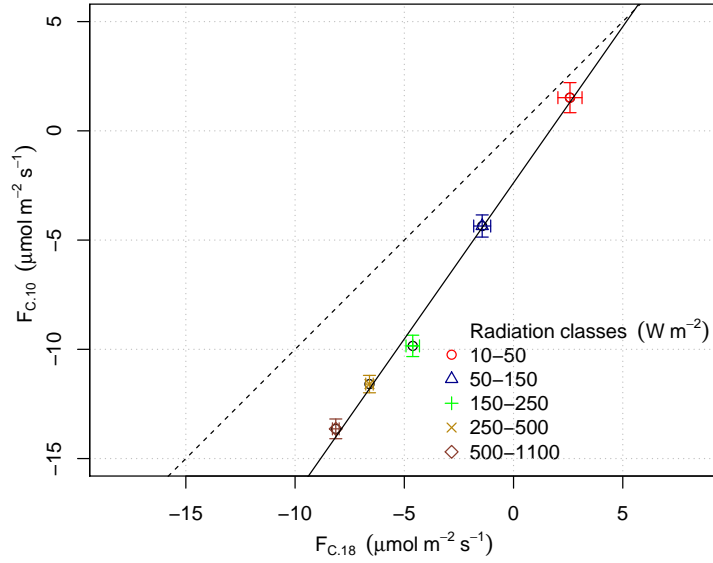


Figure 3.21.: Comparison of the bootstrapping-derived mean net carbon fluxes between FORKAST 2010 and GRACE 2018 in the comparison period. Arrows display the respective standard errors. The dashed line shows the 1:1 ratio, the black line is the linear regression between the two years ($p < 0.001$).

Table 3.1.: Cumulative fluxes of carbon, water and their relative deviation in the comparison period during FORKAST 2010 and GRACE 2018.

Carbon fluxes (g C m^{-2})	FORKAST	GRACE	Deviation to FORKAST (%)
NEE	-81.5	-56.3	-31
GPP	-353.5	-304.4	-14
R_{eco}	272	248.1	-9
Water fluxes (mm)			
Precipitation	240.9	68.4	-72
Evapotranspiration	40.3	57.8	+43
Surface water balance	200.6	10.6	-95

Table 3.2.: Mean daily carbon fluxes and their respective standard deviation in the comparison period during FORKAST 2010 and GRACE 2018.

Mean daily fluxes ($\text{g C m}^{-2} \text{d}^{-1}$)	FORKAST	GRACE
NEE	-1.7 ± 0.2	-1.2 ± 0.1
GPP	-7.3 ± 1.6	-6.4 ± 1.5
R_{eco}	5.6 ± 1.2	5.2 ± 0.8

3.4. Carbon flux comparison

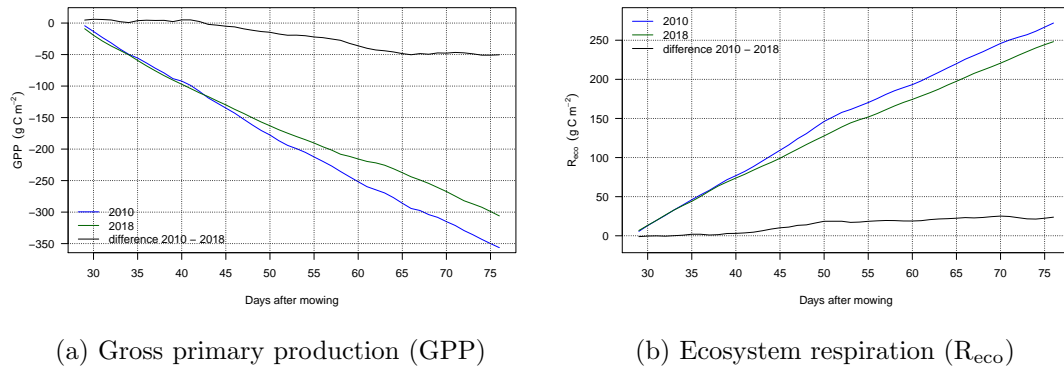


Figure 3.22.: Cumulative flux components gross primary production (GPP) and ecosystem respiration (R_{eco}) during FORKAST 2010 and GRACE 2018 in the comparison period. Results are based on daily sums.

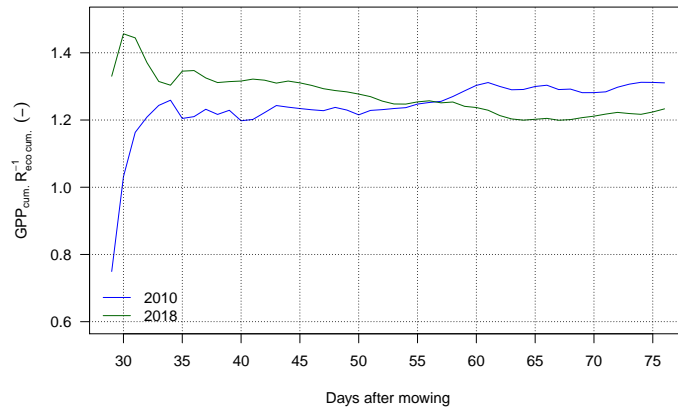


Figure 3.23.: Ratio between the cumulative sums of gross primary production (GPP) and ecosystem respiration (R_{eco}) for FORKAST 2010 and GRACE 2018 in the comparison period.

3.5. Environmental controls on carbon dioxide exchange

3.5.1. GPP in response to light and temperature

Light use efficiency revealed that light was used more efficiently for photosynthesis during FORKAST than during GRACE (fig. 3.24). Despite a lower global radiation in 2010 during the comparison period (fig. 3.11a), the resulting GPP was higher (fig. 3.22a). This results most likely from more assimilating plant matter for which no direct measurements were available. However, NDVI can be used as proxy, which ranges between 0 (no leaves) and 1 (green leaves). It showed a reduction in July and August 2018 (fig. 3.25). Due to the climatic conditions this was attributed to drought-induced senescence. Interestingly, despite the presumed difference in plant canopy conditions, light explained more than half of the variance in mean daily GPP in both years.

Moreover, GPP showed little correlation with temperature ($R^2 = 0.09$ during FORKAST and 0.40 during GRACE, data not shown).

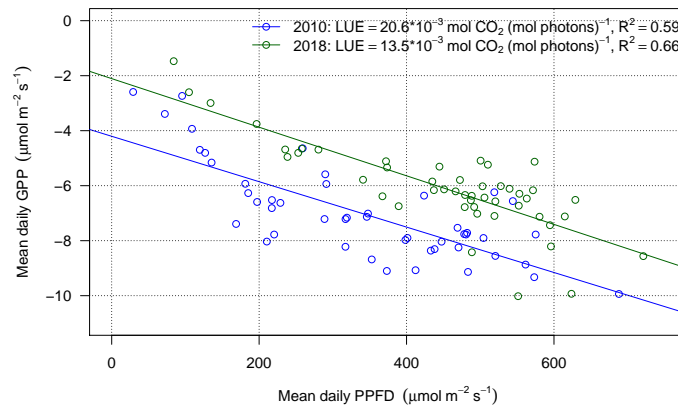


Figure 3.24.: Light use efficiency (LUE) of FORKAST 2010 and GRACE 2018 in the comparison period. Lines display the linear regressions for the respective years, both are significant ($p < 0.001$).

3.5.2. Ecosystem respiration in response to temperature and GPP

Despite the exponential model (see eq. 2.3), R_{eco} related slightly more linear to mean daily air temperature (R^2 for exponential fit is 0.91 and 0.84 during GRACE and FORKAST, respectively) during the comparison period in both years (fig. 3.26), which was presumably due to the considered temperature range. Q_{10} was higher during FORKAST, also reflected by the slope of the linear regression model. Additionally, the offset is bigger, being comparable to the bulk respiration parameter R_{10} from eq. 2.3. The higher temperatures during GRACE (fig. 3.1) did therefore not result in higher cumulative sums of respiration compared to FORKAST (fig. 3.22b).

3.5. Environmental controls on carbon dioxide exchange

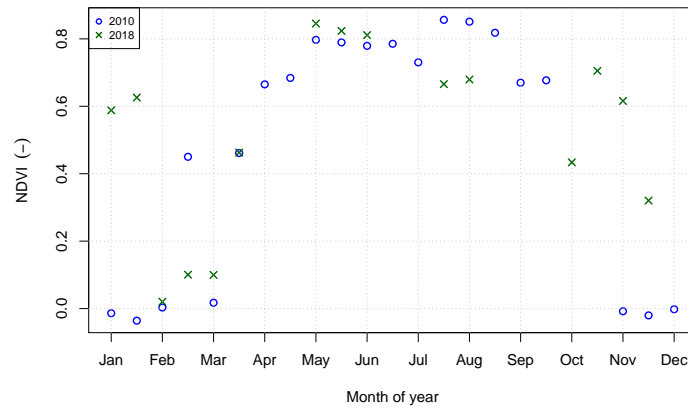


Figure 3.25.: Normalized difference vegetation index (NDVI) for the years 2010 and 2018.

Contrary, the correlation between R_{eco} and GPP was low for both years ($R^2 = 0.21$ during FORKAST and 0.36 during GRACE, data not shown).

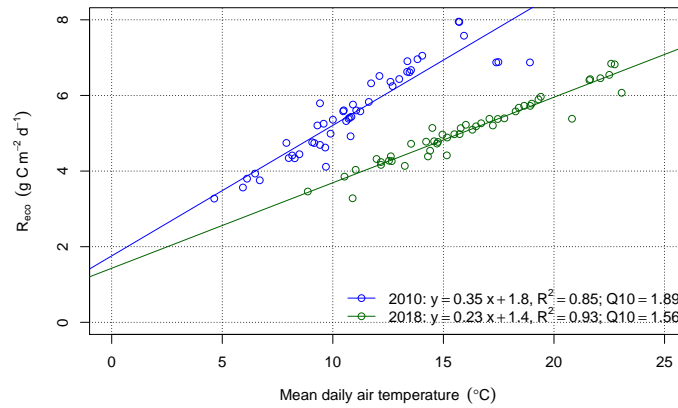


Figure 3.26.: Linear regressions of daily ecosystem respiration (R_{eco}) on mean daily air temperature for FORKAST 2010 and GRACE 2018 in the comparison period; both are significant ($p < 0.001$). Q10 values are based on exponential model (not shown).

4. Discussion

4.1. Drought influence on ecosystem CO₂ exchange

Here, drought was assessed via precipitation deficits (see figs. 3.2, 3.3), temperature anomalies (fig. 3.1), the resulting SWB (fig. 3.10b), remotely-sensed indices (fig. 3.25) and its impact on evaporative fluxes in relation to energy input ($ET \cdot ET_{pot}^{-1}$ in fig. 3.14).

The presented joint reduction of the flux components GPP and R_{eco} , caused by drought, is commonly observed across many ecosystems; the reduction of GPP is thereby usually larger than that of R_{eco} , which leads to a decreased NEE (van der Molen et al., 2011).

Turning to comparable studies, Wolf et al. (2013) showed that spring drought even increased NEE at a montane grassland site, whereas two sites at lower elevations in the study showed only minor reductions. Accordingly, Hussain et al. (2011) found annual GPP and R_{eco} to be reduced by 20% and 25% respectively, which exceeds the seasonal deviation observed in this study. Their data is obtained from the comparable, extensively managed grassland site “Grillenburg” in the well-studied drought year 2003. Interestingly, the higher relative deviation of R_{eco} compared to GPP causes the resulting NEE to be slightly higher in the drought year, which contradicts this study with its 31% NEE decrease, assessed in the second growing season. Moreover, the ratio of $GPP \cdot R_{eco}^{-1}$ equalled 1.3 for FORKAST and 1.2 for GRACE at the end of the comparison period (fig. 3.23). Therefore, R_{eco} offset more of assimilated C in the drought year, even though the absolute flux was reduced (fig. 3.22b). In other words, GPP was reduced proportionally stronger than R_{eco} . Conversely, the drought year from Hussain et al. (2011) had a higher ratio (1.4) and thus relatively higher NEE than their normal year with 1.3.

A possible reason for the opposed behaviour between the two studies is that the considered time period in the second growing season is with 48 days much shorter in the presented study than the full year study from Hussain et al. (2011). Their site has been mowed twice in the drought year and three times during the reference year. Therefore the effect of management, which temporarily reduces GPP (cf. fig. 3.4 and Zeeman et al., 2010) is included in their results and possibly biases their findings.

Conversely, the presented results match with the impacts of the summer heat 2003 found on a larger scale for Europe. Ciais et al. (2005) showed that nearly all investigated forest sites and one grassland site significantly reduced the absolute values of GPP and NEE. For total Europe, the authors found a substantial reduction of primary productivity by 30%. In agreement, significant NEE reductions are reported by Ammann et al. (2007) for two temperate grassland sites, confirming the described drought impact observed during GRACE.

In the following, the role of the flux components GPP and R_{eco} is further elaborated. Moreover, their reaction to the main environmental drivers is compared.

4.1.1. Gross primary production

The smaller GPP is expected to result from moisture limitations, as inferred from the negative SWB and low $ET \cdot ET_{pot}^{-1}$ values in the comparison period during GRACE. Subsequently, aboveground biomass is expected to be less developed than during FORKAST. These two interconnected parameters, soil moisture and aboveground biomass, have been shown to exert a major control on GPP (e.g. Wohlfahrt et al., 2008a).

Furthermore, light explained a large part of the variation in GPP (fig. 3.24) in both years. This agrees with Wohlfahrt et al. (2008b) who synthesized flux measurements from nine grassland sites. However, at Mediterranean sites with a pronounced summer drought, the variance explained by light decreased and thus showed a moisture dependency. This is not the case in the presented comparison, contrary, GPP correlated stronger with light in the drought year, possibly due to the more constant radiative input (fig. 3.11).

However, LUE reduced due to drought which has also been reported by Hussain et al. (2011). The absolute values of LUE are not directly compared to other studies, since PFD in the presented study is not based on measurements, but derived from using a fixed conversion factor (see chap. 2.6.2). However, since the resulting values are used for the comparison of two years, they do not have to be accurate. Gilmanov et al. (2007) showed that LUE decreases with a reduced amount of assimilating plant matter, as it is the case after mowing events. Thus, less assimilating biomass can be inferred for GRACE, resulting from drought instead from management (see also NDVI in fig. 3.25).

4.1.2. Ecosystem respiration

Similarly to GPP, R_{eco} was reduced in response to drought (figs. 3.22b, 3.26). Despite of its smaller magnitude of decrease (Table 3.1), this component plays an important role in the balance because of the multiple, interacting drivers involved in it. The respiratory flux from soil (i.e. root respiration and respiration from soil organisms) has been shown to decrease under drought stress (Joos et al., 2010; Xu et al., 2004).

Autotrophic respiration was likely reduced due to less plant biomass as inferred from the NDVI (fig. 3.25), which again influences soil respiration through less assimilate supply. The latter has been shown to be a main driver for soil respiration in grasslands (Bahn et al., 2008). However, the low correlation between R_{eco} and GPP questions the transferability to the presented data. Due to the results from Riederer et al. (2015), the observed reduction of R_{eco} can be mainly attributed to reduced shoot (hence autotrophic) respiration. This respiratory component has been shown to double soil respiration under non water-limited conditions by means of an isotope labeling experiment at the study site.

Temperature, via its usually exponential influence on enzyme kinetics (see also eq. 2.3), correlated strongly with R_{eco} in both experiments, which well agrees with other studies (e.g. Wohlfahrt et al., 2005a, 2008a). Notably, the temperature sensitivity decreased during GRACE. In line with this, Hussain et al. (2011) showed that Q_{10} decreased under low soil moisture conditions (similarly found by Wohlfahrt et al., 2008a; Xu and Baldocchi, 2004).

The observed behaviour of R_{eco} underscores that higher temperatures do not necessarily translate into higher C turnover. Instead, the effect of soil moisture has to be taken into

account in order to accurately assess the reaction of this component under changing climatic conditions. For example, Ruehr et al. (2010) showed for forest soils that the dependency of respiration on temperature is lost under low soil moisture conditions. At the site, it is expected that respiratory fluxes decrease under drought, which alleviates the NEE-reduction caused by the more obviously reduced GPP. However, by means of the ratio $GPP \cdot R_{eco}^{-1}$, it was shown that despite the absolute reduction of R_{eco} , more of the assimilated C was offset during GRACE. This dampened the NEE-reduction but did not compensate for it.

It can be further shown that not the relation to the environmental drivers changed (reflected by the R^2 -values in figs. 3.24, 3.26), but the response to them, as reflected by the light and temperature response.

4.1.3. Net ecosystem exchange

The comparison of the cumulative NEE fluxes is based on a rather short time period and about half of the comparison period, the NEE difference is close to zero. What causes the NEE-reduction during GRACE and what is the role of the environmental drivers?

The difference between the two years mainly originates from increased uptake during FORKAST and decreased uptake during GRACE. During FORKAST, NEE peaked at the days 57 - 61, after an exceptionally high rainfall event (fig. 3.10a). It could be presumed that the subsequent well-watered conditions favour C uptake. The tight coupling between precipitation and NEE was found on an annual time-scale (Chou et al., 2008; Knapp et al., 2002). However, in the total comparison period, the SWB is well above zero, hence relieved drought stress is unlikely. Additionally, global radiation reached similar values in the preceding days, however, the strong response in NEE was lacking. Contrary, mean daily temperature dropped to low values during the considered days (fig. 3.11a). Since FORKAST showed a high temperature sensitivity (fig. 3.26), R_{eco} was significantly reduced. At the same time, the less temperature-dependent GPP was sustained by high radiative input (fig. 3.24), hence NEE was increased.

NEE of GRACE kept up with FORKAST for half of the comparison period, even under drought stress, as inferred from the negative SWB (fig. 3.9). This resulted from high global radiation (fig. 3.11b), favouring GPP and relatively low C losses (fig. 3.26). Despite the high values of global radiation between the days 55 - 58, net uptake was only weakly increased, which can be attributed to the still negative water balance (fig. 3.10b), likely resulting in soil moistures below wilting point. The site turned into a net source for a short time (days 62 - 64) when both, global radiation and water balance were low (fig. 3.11b); it then recovered to a net sink after rainfall and higher radiation at day 66. Note that day 55 refers to 26.08.2018, being two days before the date of fig. A.3c on which one can distinctly recognize dried out patches. Also the color scale in fig. 3.8 indicates reduced NEE fluxes.

By means of fig. 3.21, the factor light was disentangled from other environmental controls on NEE. In the same radiation classes, FORKAST showed higher net fluxes, demonstrating that the light conditions did not cause the difference in NEE. The same has been shown for the component GPP (fig. 3.24). Hence, the drought effect on C fluxes

was not veiled by differences in radiation. For GRACE, the drought impact on GPP via reducing LUE is seen as the governing control, which finally reduced NEE. It is expected that under the same light regime as GRACE, FORKAST would have shown even higher NEE.

During FORKAST, low temperatures (fig. 3.18) reduced R_{eco} (fig. 3.26) while at the same time high global radiation caused GPP to increase (figs. 3.22a, 3.24) which led to an increase of NEE (fig. 3.21).

4.2. Drought influence on energy exchange

4.2.1. Energy fluxes

Cumulative sums of ET and the SWB in the comparison period differed considerably (fig. 3.10, Table 3.1). Considering the precipitation deficits during GRACE, lower ET would have been expected due to water limitation. However, atmospheric water demand was higher during GRACE due to higher global radiation (fig. 3.11), higher temperatures, higher VPD and thus higher ET_{pot} . This led to a higher ET sum and resulted in even enhanced drought stress, since not only precipitation and with this soil moisture recharge was less, but also more water evaporated.

Since the SWB was partly negative during GRACE (fig. 3.9), it is concluded that soil moisture supplied ET and thus was gradually depleted. Conversely, during FORKAST (fig. 3.10a), more of the precipitation is expected to infiltrate and hence was available as soil moisture for plant growth, as reflected by the positive SWB.

Regarding the directly compared ET (fig. 3.12), both years showed approximately equal fluxes per radiation class. Contrary for GRACE, water limitation was evident in the ratio $ET \cdot ET_{pot}^{-1}$ (fig. 3.14), whereas FORKAST had, besides some scatter, values close to one, showing that actual ET was able to fulfil the atmospheric demand. Therefore, ET in the latter experiment was energy limited, whereas GRACE showed water limitation. The absolute values of ET per radiation class were approximately maintained, whereas the relative proportion to the energy input, partly expressed via ET_{pot} , decreased during GRACE. Concomitantly, more energy was translated to sensible heat flux, which is shown by means of the Bowen-ratio (fig. 3.16). However, by virtue of the high ET, sensible heat fluxes stayed at moderate levels, alleviating the temperature increase caused by the increased energy input (see also Teuling et al., 2010).

Wolf et al. (2013) observed no impact or in one case slightly increased ET during spring drought at three grassland sites, which partly agrees with the presented results.

The findings from Hammerle et al. (2008) at a temperate mountain grassland show that the presence of plant matter, expressed as green area index, is an important biotic influence factor for ET, since canopy conductance is expected to increase the transpiration component of ET. They also found VPD to be an important abiotic driver for ET. Since the presented results showed higher ET in the drought year GRACE with less developed plant biomass (NDVI in fig. 3.25), the abiotic influence factors (global radiation, VPD) outweigh the biotic ones.

In general, albedo plays an important role for the partitioning of energy fluxes. The

higher values measured during FORKAST (fig. 3.17) can be explained by higher above-ground biomass (fig. 3.25), which falls well in line with Hammerle et al. (2008). The authors explain the increase via less contribution of the soil reflectance and an increased contribution from the near-infrared band of the canopy. Accordingly, grass cuts led to a decreased albedo in their study, which can also be recognized in the measurements from 2018 (fig. 3.17b). Again, this supports the NDVI-based assumption of less developed biomass during GRACE.

Additionally, the authors question the representativeness of moisture measurements in the upper soil layer, since deeper roots, even if small in mass, might significantly contribute to water uptake (see also Miller et al., 2007, who measured soil moisture at different depths). This might also explain why despite a negative SWB which followed an already dry spring, plant water demand was fulfilled and hence C uptake was still sustained. Moreover, the variability in plant canopy conditions visually observed in Voitsumra could be attributed to different rooting depths. End of August, GRACE showed patches being virtually dried out (fig. A.3d) with a canopy height of only 3 cm. Contrary, patches east of the AWS showed well developed biomass (fig. A.3e) and a canopy height of 12 cm. This difference might also result from spatially variable soil moisture patterns.

4.2.2. Water use efficiency

A lower WUE has been found for the drought experiment GRACE than for FORKAST (fig. 3.15). The opposite would have been expected, since adaption to drought often leads to an increased WUE in order to minimize water loss (for forests see e.g. Thomas et al., 2009). The study from Hussain et al. (2011) found a slight increase in inherent WUE during the 2003 drought year, which represents the common expectation. Conversely, no change in WUE has been reported by Wolf et al. (2013) for three grassland sites experiencing a spring drought. However in the drought year of their study, ET remained approximately the same at two sites, whereas GPP either decreased, stayed constant or increased at the sites. This impedes a direct comparison to the presented study.

Notably, the drought conditions reduced LUE during GRACE (fig. 3.24 for GPP and fig. 3.21 for NEE), whereas Q_e was approximately maintained in the respective radiation classes (fig. 3.12) and increased with regard to the cumulative sum (fig. 3.9). With this, the reduction of WUE can be mainly traced back to the reduced GPP. Additionally, WUE depends on global radiation, since ET is theoretically unlimited whereas GPP follows a saturation type function (see eq. 2.2). Since the radiative input of the two comparison periods differed, WUE might be biased.

The relatively short grassland canopy is close to the bare soil; hence WUE, ideally representing the ratio between GPP and water loss by transpiration (Beer et al., 2009) is stronger influenced by soil evaporation than it is the case in forests. Additionally, the chosen trade-off between the exclusion of rainy days and data availability causes ET to be influenced by bare soil evaporation and interception. Moreover, the variance of GPP explained by ET was low for both years, likely showing a low coupling between the C and water fluxes at the site.

It was initially attempted to calculate inherent WUE, however GPP multiplied by mean

daylight VPD had little correlation with ET (data not shown). Beer et al. (2009) explain this by presuming that the underlying approximation of $e_i - e_a \approx vpd$ is invalid; e denotes water vapour pressure, the indices i and a refer to inner and ambient, respectively. This again shows that the stomata control might be minor at grassland sites.

4.3. Uncertainty evaluation

4.3.1. Measurement uncertainty

As described in chapter 2.3.2, no footprint analysis has been performed due to the small differences in the ensemble average cycles. This does however not imply that a footprint from the neighbouring site is non-existent, but the resulting error is assumed to be small compared to the uncertainty which would have been introduced by replacing the data with modelled fluxes.

Radiation measurements at the AWS might not be representative for the site, as can be seen in fig. A.3b. The brighter ground underneath the sensor is due to the later mowing of the AWS-plot, which was done on 18.07.2018. It was expected that albedo is higher due to the brighter ground, however this was not found in the data. Indeed, albedo decreased in response to cutting (fig. 3.17b, see also chapter 4.2.1). Therefore, albedo might be biased to lower values in 2018. Nevertheless, the surrounding site is expected to be represented in the measurements, since the radiation sensor captures a broad angular perspective. According to Foken (2016) (referring to Latimer, 1971), the sensor height at 2 m captures 90% of its measurements from a circle of 12 m diameter, which distinctly exceeds the area of the AWS.

Q_s^* of 2010 had to be partly parametrised due to missing data (chapter A.2.1), which translates to smaller uncertainties in the gap-filled ET of this year (fig. 3.10a). However, this was accounted for by solely using measured and approved data for the direct flux comparison (fig. 3.12) and for the drought indicator $ET \cdot ET_{pot}^{-1}$ (fig. 3.14). Further, the missing radiative fluxes limit our analyses of ET and NEE grouped in radiative fluxes (figs. 3.12, 3.21), in which global radiation is used. Given the observed albedo changes (fig. 3.17), a consideration of the net short-wave radiation would have been more appropriate. Additionally, the difference in global radiation between FORKAST and GRACE (fig. 3.11) is expected to be also seen in Q_s^* . In order to gain a more detailed understanding of the energy flux partitioning at the site, displaying the energy fluxes in relation to Q_s^* would have represented an interesting analysis (similar to Hammerle et al., 2008).

Causes (precipitation anomalies) and impacts (on fluxes) are considered in this work for the assessment of drought. Soil moisture would have been a rewarding complementary measurement, since it provides the direct link of drought impacts on plant water use (van der Molen et al., 2011). For example, Jaksic et al. (2006) compared NEE of a grassland in years with contrasting precipitation sums. The wet year showed even less NEE and the authors concluded that the observed small difference cannot be attributed to drought stress, since soil moisture was always above wilting point. Nevertheless the presented results, especially the changes in LUE and temperature sensitivity are in accordance with other studies. Hence, the reaction of the fluxes supports the underlying

assumption of water deficiencies. At the Voitsumra site, moisture sensors would have been ideally installed at several depths along the rooting zone, since the deeper soil horizons often contain more water (Miller et al., 2007, and chapter 4.2.1). However, the spatial variability visually observed at the site (e.g. figs. A.3e, A.3d) would have been difficult to cover.

A quantitative measure for the amount of aboveground biomass would have been suitable for explaining GPP. For example, Wohlfahrt et al. (2008a) achieved this by relating GPP to green area index. In the presented work, NDVI is used as a proxy for assessing the condition of the vegetation canopy, however, the data quality is not always adequate (see also chapter 2.2.3). For example, NDVI in October 2018 is slightly above 0.4. However, the site had well developed biomass at this time (fig. A.3g) which questions the usefulness of the parameter.

Additionally, knowledge of the harvest output from the first grass cut in 2018 would have enabled a direct comparison to the one in 2010, representing a direct measure for the amount of aboveground biomass. This could have served as an additional indicator for drought impacts. Aboveground biomass is tightly coupled to NEE, since the largest part of the assimilated C was found in shoots again (Riederer et al., 2015).

4.3.2. Modelling uncertainty

GPP results from the difference between measured or modelled NEE and modelled R_{eco} (see chapter 2.4). During daytime, NEE is mostly based on measurements. Contrary, daytime R_{eco} is always based on modelling by extrapolating the Lloyd-Taylor fit with approved nighttime data to daytime temperatures. With this, any uncertainty which results from the simple Lloyd-Taylor model is translated to daytime GPP. Since drought influenced the temperature sensitivity of R_{eco} (see chapter 4.1.2), also GPP will be reduced. Solely measured and approved data have been analysed for the direct net flux comparisons (fig. 3.21 and 3.12), which support the presented findings. Therefore, the uncertainty from modelling can be regarded as insignificant.

The linear model in fig. 3.24 does not correspond to the hyperbolic model performed by the Michaelis-Menten equation (see eq. 2.2) or similarly detected relationships (e.g. Wohlfahrt et al., 2008a). It thus only represents an approximation of the relationship between the two variables.

Additionally, foliar respiration can be reduced in light compared to nighttime conditions. Since the Lloyd-Taylor fit (eq. 2.3) is based on nighttime data, modelled daytime R_{eco} and with this GPP might be overestimated. Wohlfahrt et al. (2005b) quantified this effect with a modelling study for a mountain meadow and suggested that GPP might be reduced by 11 - 17%.

4.3.3. Drought assessment

The comparison period (see chapter 2.7) captures only part of the year 2018 and therein only a fraction of the second growing period following the first cut. This neglects the precipitation deficits which were already present in February (fig. 3.2). Moreover, possible

carry-over effects from spring and early summer cannot be accounted for. Accordingly, it has been reported that vegetation regrowth following grass cuts was strongly inhibited by soil moisture limitations (Wolf et al., 2013; Hussain et al., 2011). Linking to this, a comparison of the mowing aftermath of the two experiments would expand the understanding of drought impacts in Voitsumra.

Prerequisite for the assessment of drought impacts is a climatically normal reference (similarly performed by Ciais et al., 2005; Hussain et al., 2011; Wolf et al., 2013). Regarding annual precipitation, the year 2010 fulfils this requirement (fig. 3.2). Contrary, the sum in August 2010, which falls in the comparison period, exceeded the mean significantly. This aggravates the comparison, since overcast skies reduced global radiation (fig. 3.11a). Additionally, water excess might impact NEE and its underlying components in a different way than under normal conditions. Also mean annual temperature fell below average in 2010 (fig. 3.1), however the influence on the comparison period is small, since the difference mainly originated from the below-average cold winter months.

Moreover, soil heat flux, which is used in the gap-filling procedure of ET has not been measured, but only been estimated to be 10% of Q_s^* (eq. 2.4). Regarding the difference in radiative input (fig. 3.11), it is expected that this component is larger in 2018. Hammerle et al. (2008) showed that soil heat flux decreased with increasing plant biomass, which conversely would reduce this flux in 2018 under the assumption of less aboveground biomass (fig. 3.25). Thus, in order to thoroughly assess the drought impact on energy fluxes, this component would have displayed a valuable measure.

5. Conclusion

This study demonstrates that the exceptional climatic conditions in 2018 suppressed C fluxes in the second growing season at a submontane grassland site (cf. figs. 3.20, 3.22 and Table 3.1) in comparison to the climatically normal year 2010. The grassland's NEE was reduced by 31% in the comparison period, resulting from both, reduced GPP and R_{eco} . These components changed the response to their main environmental drivers, such that LUE (fig. 3.24) and the temperature sensitivity (fig. 3.26) decreased.

Conversely, energy fluxes increased in response to the higher energy input (fig. 3.11) at the site. Soil moisture supplied the high atmospheric water demand and the cumulative sum of ET therefore exceeded the reference year (fig. 3.10). Nevertheless, water limitations were obvious in the SWB and the ratio $ET \cdot ET_{\text{pot}}^{-1}$ (fig. 3.14). Additionally, the Bowen-ratio indicated that more energy was shifted to sensible heat flux during the drought year (fig. 3.16), however, the high ET still dampened surface heating.

This highlights the detrimental impact of climate extremes on the C balance of ecosystems, potentially turning them into C sources. Climate extremes hence have the potential to result in a positive feedback to climate change. Furthermore, the findings challenge the understanding of environmental drivers and show that simple predictions from current relationships are not reasonable, because the response to them is modified under drought. However, the site dampened drought impacts, since GPP reductions were partly compensated by the reduced R_{eco} and a high regrowth potential of the biomass in the remainder of the growing season. Additionally, surface heating was suppressed, since ET increased in response to the higher energy input.

Future management strategies should carefully consider the trade-off between economic use and a prolonged growing season by less frequent management. At the investigated site, this helped to compensate for deficits in C uptake of the drought year during the second growing period (fig. 3.19).

Bibliography

- Aires, L. M. I., Pio, C. A., and Pereira, J. S.: Carbon dioxide exchange above a Mediterranean C3/C4 grassland during two climatologically contrasting years, *Global Change Biology*, 14, 539–555, 2008.
- Ammann, C., Flechard, C., Leifeld, J., Neftel, A., and Fuhrer, J.: The carbon budget of newly established temperate grassland depends on management intensity, *Agriculture, Ecosystems & Environment*, 121, 5–20, 2007.
- Bahn, M., Rodeghiero, M., Anderson-Dunn, M., Dore, S., Gimeno, C., Drösler, M., Williams, M., Ammann, C., Berninger, F., Flechard, C., et al.: Soil respiration in European grasslands in relation to climate and assimilate supply, *Ecosystems*, 11, 1352–1367, 2008.
- Baldocchi, D., Falge, E., Gu, L., Olson, R., Hollinger, D., Running, S., Anthoni, P., Bernhofer, C., Davis, K., Evans, R., et al.: FLUXNET: A new tool to study the temporal and spatial variability of ecosystem-scale carbon dioxide, water vapor, and energy flux densities, *Bulletin of the American Meteorological Society*, 82, 2415–2434, 2001.
- Baldocchi, D. D.: Assessing the eddy covariance technique for evaluating carbon dioxide exchange rates of ecosystems: past, present and future, *Global change biology*, 9, 479–492, 2003.
- Battin, T. J., Luyssaert, S., Kaplan, L. A., Aufdenkampe, A. K., Richter, A., and Tranvik, L. J.: The boundless carbon cycle, *Nature Geoscience*, 2, 598, 2009.
- Beer, C., Ciais, P., Reichstein, M., Baldocchi, D., Law, B., Papale, D., Soussana, J.-F., Ammann, C., Buchmann, N., Frank, D., et al.: Temporal and among-site variability of inherent water use efficiency at the ecosystem level, *Global biogeochemical cycles*, 23, 2009.
- Berry, P., Smith, A., Eales, R., Papadopoulou, L., Erhard, M., Meiner, A., Bastrup-Birk, A., Ivits, E., Gelabert, E. R., Dige, G., et al.: Mapping and assessing the condition of Europe’s ecosystems: progress and challenges - EEA contribution to the implementation of the EU Biodiversity Strategy to 2020, EEA Report. No 3, 2016.
- Canty, A. and Ripley, B. D.: boot: Bootstrap R (S-Plus) Functions, r package version 1.3-20, 2017.
- Chou, W. W., Silver, W. L., Jackson, R. D., Thompson, A. W., and Allen-Diaz, B.: The sensitivity of annual grassland carbon cycling to the quantity and timing of rainfall, *Global Change Biology*, 14, 1382–1394, 2008.

- Ciais, P., Reichstein, M., Viovy, N., Granier, A., Ogée, J., Allard, V., Aubinet, M., Buchmann, N., Bernhofer, C., Carrara, A., et al.: Europe-wide reduction in primary productivity caused by the heat and drought in 2003, *Nature*, 437, 529, 2005.
- DAAC, N. L.: MODIS (MOD13Q1), 16 days NDVI, accessed on 19.01.2019, at <https://lpdaacsvc.cr.usgs.gov/appears>, 2018.
- Foken, T.: *Angewandte Meteorologie*, Springer-Verlag Berlin Heidelberg, 3. auflage edn., 394 Seiten, 2016.
- Foken, T., Göckede, M., Mauder, M., Mahrt, L., Amiro, B., and Munger, W.: Post-field data quality control, in: *Handbook of micrometeorology*, pp. 181–208, Springer, 2004.
- Friedrich, K. and Kaspar, F.: Rückblick auf das Jahr 2018 - das bisher wärmste Jahr in Deutschland, Tech. rep., DWD - German Weather Service, 2019.
- Gilmanov, T., Soussana, J., Aires, L., Allard, V., Ammann, C., Balzarolo, M., Barcza, Z., Bernhofer, C., Campbell, C., Cernusca, A., et al.: Partitioning European grassland net ecosystem CO₂ exchange into gross primary productivity and ecosystem respiration using light response function analysis, *Agriculture, ecosystems & environment*, 121, 93–120, 2007.
- Göckede, M., Markkanen, T., Hasager, C. B., and Foken, T.: Update of a footprint-based approach for the characterisation of complex measurement sites, *Boundary-Layer Meteorology*, 118, 635–655, 2006.
- Haase, M.: CO₂ - Flüsse über einer Wiesenfläche im Fichtelgebirge; Dokumentation des mikrometeorologischen Experiments in Voitsumra, Tech. rep., Universität Bayreuth - Abteilung Mikrometeorologie, 2010.
- Hammerle, A., Haslwanter, A., Tappeiner, U., Cernusca, A., and Wohlfahrt, G.: Leaf area controls on energy partitioning of a temperate mountain grassland, *Biogeosciences* (online), 5, 2008.
- Houghton, J. T., Ding, Y., Griggs, D. J., Noguera, M., van der Linden, P. J., Dai, X., Maskell, K., and Johnson, C.: *Climate change 2001: the scientific basis*, The Press Syndicate of the University of Cambridge, 2001.
- Hussain, M., Grünwald, T., Tenhunen, J., Li, Y., Mirzae, H., Bernhofer, C., Otieno, D., Dinh, N., Schmidt, M., Wartinger, M., et al.: Summer drought influence on CO₂ and water fluxes of extensively managed grassland in Germany, *Agriculture, ecosystems & environment*, 141, 67–76, 2011.
- Jaksic, V., Kiely, G., Albertson, J., Oren, R., Katul, G., Leahy, P., and Byrne, K. A.: Net ecosystem exchange of grassland in contrasting wet and dry years, *Agricultural and Forest Meteorology*, 139, 323–334, 2006.

- Joos, O., Hagedorn, F., Heim, A., Gilgen, A. K., Schmidt, M., Siegwolf, R., and Buchmann, N.: Summer drought reduces total and litter-derived soil CO₂ effluxes in temperate grassland—clues from a 13 C litter addition experiment, *Biogeosciences*, 7, 1031–1041, 2010.
- Keenan, T. F., Hollinger, D. Y., Bohrer, G., Dragoni, D., Munger, J. W., Schmid, H. P., and Richardson, A. D.: Increase in forest water-use efficiency as atmospheric carbon dioxide concentrations rise, *Nature*, 499, 324, 2013.
- Knapp, A. K., Fay, P. A., Blair, J. M., Collins, S. L., Smith, M. D., Carlisle, J. D., Harper, C. W., Danner, B. T., Lett, M. S., and McCarron, J. K.: Rainfall variability, carbon cycling, and plant species diversity in a mesic grassland, *Science*, 298, 2202–2205, 2002.
- Latimer, J.: Radiation Measurement: International Field Year for the Great Lakes, Canadian National Committee for the International Hydrological Decade, 1971.
- Le Quéré, C., Raupach, M. R., Canadell, J. G., Marland, G., Bopp, L., Ciais, P., Conway, T. J., Doney, S. C., Feely, R. A., Foster, P., et al.: Trends in the sources and sinks of carbon dioxide, *Nature geoscience*, 2, 831, 2009.
- Lloyd, J. and Taylor, J.: On the temperature dependence of soil respiration, *Functional ecology*, pp. 315–323, 1994.
- Loos, E.: Bachelor thesis: Dynamics of the temperature and wind profiles in the boundary layer of a valley in the Fichtelgebirge Mountains, 2016.
- Marcolla, B., Cescatti, A., Manca, G., Zorer, R., Cavagna, M., Fiora, A., Gianelle, D., Rodeghiero, M., Sottocornola, M., and Zampedri, R.: Climatic controls and ecosystem responses drive the inter-annual variability of the net ecosystem exchange of an alpine meadow, *Agricultural and forest meteorology*, 151, 1233–1243, 2011.
- Mauder, M. and Foken, T.: Documentation and instruction manual of the eddy-covariance software package TK3 (update), 2015.
- McCree, K. J.: Test of current definitions of photosynthetically active radiation against leaf photosynthesis data, *Agricultural Meteorology*, 10, 443–453, 1972.
- McKee, T. B., Doesken, N. J., Kleist, J., et al.: The relationship of drought frequency and duration to time scales, in: *Proceedings of the 8th Conference on Applied Climatology*, vol. 17, pp. 179–183, American Meteorological Society Boston, MA, 1993.
- Menten, L. and Michaelis, M.: Die Kinetik der Invertinwirkung, *Biochem Z*, 49, 333–369, 1913.
- Miller, G. R., Baldocchi, D. D., Law, B. E., and Meyers, T.: An analysis of soil moisture dynamics using multi-year data from a network of micrometeorological observation sites, *Advances in Water Resources*, 30, 1065–1081, 2007.

- Moore, C.: Frequency response corrections for eddy correlation systems, *Boundary-Layer Meteorology*, 37, 17–35, 1986.
- Nagy, Z., Pintér, K., Czóbel, S., Balogh, J., Horváth, L., Fóti, S., Barcza, Z., Weidinger, T., Csintalan, Z., Dinh, N., et al.: The carbon budget of semi-arid grassland in a wet and a dry year in Hungary, *Agriculture, Ecosystems & Environment*, 121, 21–29, 2007.
- Pachauri, R. K., Allen, M. R., Barros, V. R., Broome, J., Cramer, W., Christ, R., Church, J. A., Clarke, L., Dahe, Q., Dasgupta, P., et al.: *Climate change 2014: synthesis report. Contribution of Working Groups I, II and III to the fifth assessment report of the Intergovernmental Panel on Climate Change*, Ipcc, 2014.
- Phoenix, G. K., Booth, R. E., Leake, J. R., Read, D. J., Grime, J. P., and Lee, J. A.: Effects of enhanced nitrogen deposition and phosphorus limitation on nitrogen budgets of semi-natural grasslands, *Global Change Biology*, 9, 1309–1321, 2003.
- Polley, H. W., Phillips, R. L., Frank, A. B., Bradford, J. A., Sims, P. L., Morgan, J. A., and Kiniry, J. R.: Variability in light-use efficiency for gross primary productivity on Great Plains grasslands, *Ecosystems*, 14, 15–27, 2011.
- Priestley, C. and Taylor, R.: On the assessment of surface heat flux and evaporation using large-scale parameters, *Monthly weather review*, 100, 81–92, 1972.
- R Core Team: *R: A Language and Environment for Statistical Computing*, R Foundation for Statistical Computing, Vienna, Austria, URL <https://www.R-project.org/>, 2018.
- Reichstein, M., Bahn, M., Ciais, P., Frank, D., Mahecha, M. D., Seneviratne, S. I., Zscheischler, J., Beer, C., Buchmann, N., Frank, D. C., et al.: Climate extremes and the carbon cycle, *Nature*, 500, 287, 2013.
- Riederer, M.: *Carbon fluxes of an extensive meadow and attempts for flux partitioning*, Ph.D. thesis, Faculty of Biology, Chemistry and Geosciences, University of Bayreuth, 2014.
- Riederer, M., Pausch, J., Kuzyakov, Y., and Foken, T.: Partitioning NEE for absolute C input into various ecosystem pools by combining results from eddy-covariance, atmospheric flux partitioning and ^{13}C pulse labeling, *Plant and Soil*, 390, 61–76, 2015.
- RStudio Team: *RStudio: Integrated Development Environment for R*, RStudio, Inc., Boston, MA, URL <http://www.rstudio.com/>, 2016.
- Ruehr, N. K., Knohl, A., and Buchmann, N.: Environmental variables controlling soil respiration on diurnal, seasonal and annual time-scales in a mixed mountain forest in Switzerland, *Biogeochemistry*, 98, 153–170, 2010.
- Ruppert, J., Mauder, M., Thomas, C., and Lüers, J.: Innovative gap-filling strategy for annual sums of CO_2 net ecosystem exchange, *Agricultural and Forest Meteorology*, 138, 5–18, 2006.

- Schär, C., Vidale, P. L., Lüthi, D., Frei, C., Häberli, C., Liniger, M. A., and Appenzeller, C.: The role of increasing temperature variability in European summer heatwaves, *Nature*, 427, 332, 2004.
- Schmitt, M., Bahn, M., Wohlfahrt, G., Tappeiner, U., and Cernusca, A.: Land use affects the net ecosystem CO₂ exchange and its components in mountain grasslands, *Biogeosciences (Online)*, 7, 2297, 2010.
- Schotanus, P., Nieuwstadt, F., and De Bruin, H.: Temperature measurement with a sonic anemometer and its application to heat and moisture fluxes, *Boundary-Layer Meteorology*, 26, 81–93, 1983.
- Scurlock, J. and Hall, D.: The global carbon sink: a grassland perspective, *Global Change Biology*, 4, 229–233, 1998.
- Soussana, J., Allard, V., Pilegaard, K., Ambus, P., Amman, C., Campbell, C., Ceschia, E., Clifton-Brown, J., Czóbel, S., Domingues, R., et al.: Full accounting of the greenhouse gas (CO₂, N₂O, CH₄) budget of nine European grassland sites, *Agriculture, Ecosystems & Environment*, 121, 121–134, 2007.
- Teuling, A. J., Seneviratne, S. I., Stöckli, R., Reichstein, M., Moors, E., Ciais, P., Luysaert, S., Van Den Hurk, B., Ammann, C., Bernhofer, C., et al.: Contrasting response of European forest and grassland energy exchange to heatwaves, *Nature Geoscience*, 3, 722, 2010.
- Thomas, C. K., Law, B. E., Irvine, J., Martin, J. G., Pettijohn, J. C., and Davis, K. J.: Seasonal hydrology explains interannual and seasonal variation in carbon and water exchange in a semiarid mature ponderosa pine forest in central Oregon, *Journal of Geophysical Research: Biogeosciences*, 114, 2009.
- Turner, D. P., Urbanski, S., Bremer, D., Wofsy, S. C., Meyers, T., Gower, S. T., and Gregory, M.: A cross-biome comparison of daily light use efficiency for gross primary production, *Global Change Biology*, 9, 383–395, 2003.
- van der Molen, M. K., Dolman, A. J., Ciais, P., Eglin, T., Gobron, N., Law, B. E., Meir, P., Peters, W., Phillips, O. L., Reichstein, M., et al.: Drought and ecosystem carbon cycling, *Agricultural and Forest Meteorology*, 151, 765–773, 2011.
- Vickers, D. and Mahrt, L.: Quality control and flux sampling problems for tower and aircraft data, *Journal of atmospheric and oceanic technology*, 14, 512–526, 1997.
- Webb, E. K., Pearman, G. I., and Leuning, R.: Correction of flux measurements for density effects due to heat and water vapour transfer, *Quarterly Journal of the Royal Meteorological Society*, 106, 85–100, 1980.
- Wilson, J. B., Peet, R. K., Dengler, J., and Pärtel, M.: Plant species richness: the world records, *Journal of vegetation Science*, 23, 796–802, 2012.

- Wohlfahrt, G., Anfang, C., Bahn, M., Haslwanter, A., Newesely, C., Schmitt, M., Drösler, M., Pfadenhauer, J., and Cernusca, A.: Quantifying nighttime ecosystem respiration of a meadow using eddy covariance, chambers and modelling, *Agricultural and Forest Meteorology*, 128, 141–162, 2005a.
- Wohlfahrt, G., Bahn, M., Haslwanter, A., Newesely, C., and Cernusca, A.: Estimation of daytime ecosystem respiration to determine gross primary production of a mountain meadow, *Agricultural and Forest Meteorology*, 130, 13–25, 2005b.
- Wohlfahrt, G., Anderson-Dunn, M., Bahn, M., Balzarolo, M., Berninger, F., Campbell, C., Carrara, A., Cescatti, A., Christensen, T., Dore, S., et al.: Biotic, abiotic, and management controls on the net ecosystem CO₂ exchange of European mountain grassland ecosystems, *Ecosystems*, 11, 1338–1351, 2008a.
- Wohlfahrt, G., Hammerle, A., Haslwanter, A., Bahn, M., Tappeiner, U., and Cernusca, A.: Seasonal and inter-annual variability of the net ecosystem CO₂ exchange of a temperate mountain grassland: Effects of weather and management, *Journal of Geophysical Research: Atmospheres*, 113, 2008b.
- Wolf, S., Eugster, W., Ammann, C., Häni, M., Zielis, S., Hiller, R., Stieger, J., Imer, D., Merbold, L., and Buchmann, N.: Contrasting response of grassland versus forest carbon and water fluxes to spring drought in Switzerland, *Environmental Research Letters*, 8, 035007, 2013.
- Xu, L. and Baldocchi, D. D.: Seasonal variation in carbon dioxide exchange over a Mediterranean annual grassland in California, *Agricultural and Forest Meteorology*, 123, 79–96, 2004.
- Xu, L., Baldocchi, D. D., and Tang, J.: How soil moisture, rain pulses, and growth alter the response of ecosystem respiration to temperature, *Global Biogeochemical Cycles*, 18, 2004.
- Zeeman, M. J., Hiller, R., Gilgen, A. K., Michna, P., Plüss, P., Buchmann, N., and Eugster, W.: Management and climate impacts on net CO₂ fluxes and carbon budgets of three grasslands along an elevational gradient in Switzerland, *Agricultural and Forest Meteorology*, 150, 519–530, 2010.
- Zeileis, A. and Grothendieck, G.: zoo: S3 Infrastructure for Regular and Irregular Time Series, *Journal of Statistical Software*, 14, 1–27, <https://doi.org/10.18637/jss.v014.i06>, 2005.

A. Appendix

A.1. GRACE 2018

A.1.1. Instruments

Table A.1.: Calibration values of the infrared-gas analyzer LiCor7500 S/N 0270.

Date	Location	Description	Units	Target value	Actual value
26.07.18	Lab	zero CO_2	$mmol\ m^{-3}$	0	0.02
		zero H_2O	$mmol\ m^{-3}$	0	-7.4
		span CO_2	ppm	453.5	454.8
		span H_2O (dew point temperature)	$^{\circ}C$	18.0	16.54
06.11.18	Voitsumra station	zero CO_2	$mmol\ m^{-3}$	0	0.09
		zero H_2O	$mmol\ m^{-3}$	0	-4.1
		span CO_2	ppm	453.5	452.0
		span H_2O (dew point temperature)	$^{\circ}C$	4.0	4.4

A.2. Forkast 2010

A.2.1. Parametrisation of net radiation

AWS data from 2010 contained irregular gaps in the radiation components, I_{\uparrow} , K_{\uparrow} and I_{\downarrow} mainly between 01.06.2010 - 01.09.2010. However, continuous Q_s^* values are required for a gap-filled Q_e time-series (see chapter 2.4).

I_{\uparrow} was parametrised in the following steps. First, surface temperature has been calculated by means of the Stefan-Boltzmann equation (cf. Foken, 2016):

$$I_{\uparrow} = \epsilon_{IR} \cdot \sigma_{SB} \cdot T^4 \quad (A.1)$$

solving for temperature T (K) and using available I_{\uparrow} -data. ϵ_{IR} is long-wave emissivity which has been set to 1, the constant $\sigma_{SB} = 5.67 \cdot 10^{-8} \text{ W m}^{-2} \text{ K}^{-4}$. Derived values were linearly regressed on 2 m air temperature (fig. A.1).

Secondly, surface temperatures were modelled from the continuous 2 m air temperatures with the derived linear model coefficients (slope = 1.11, intercept = -0.99). Thirdly,

missing I_{\uparrow} were then calculated via eq. A.1 from the modelled surface temperatures. Comparison of modelled I_{\uparrow} and measured I_{\uparrow} (fig. A.2) yielded an appropriate root-mean-square-deviation of 12.98 W m^{-2} .

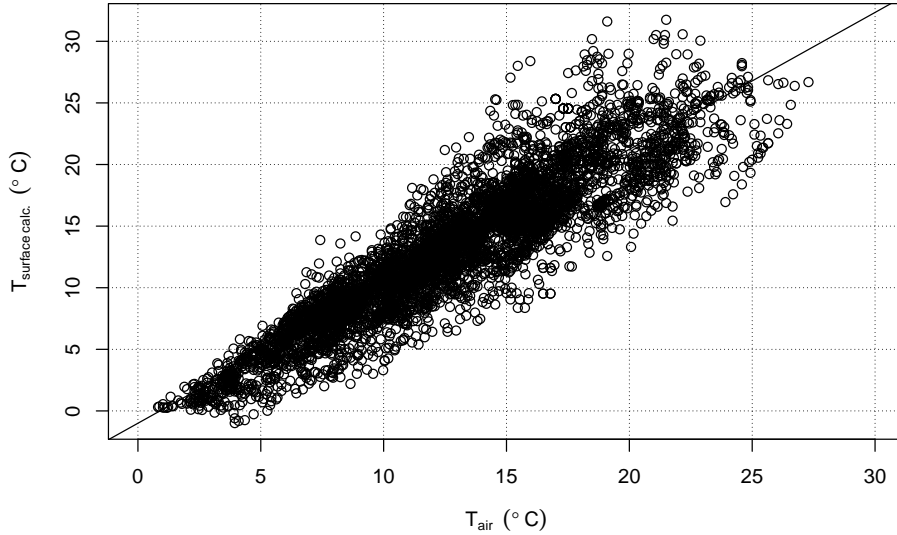


Figure A.1.: Linear regression between calculated surface temperature and measured air temperature at 2 m height in the time between 01.06.2010 - 01.09.2010. Solid line displays linear model.

From the continuous data for incoming short-wave radiation, the reflected part K_{\uparrow} was calculated with a constant albedo of 0.18 (Foken, 2016). Incoming long-wave radiation I_{\downarrow} was taken from the continuous record at the nearby flux tower “Waldstein-Weidenbrunnen”. Data from 2018 showed a good match with the measurement site in Voitsumra during daytime, which reflects the important time period for Q_e .

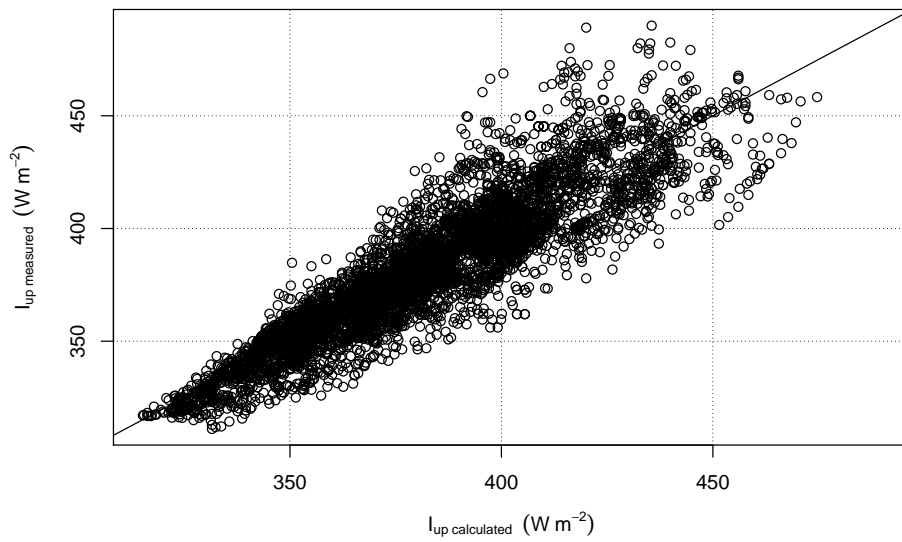
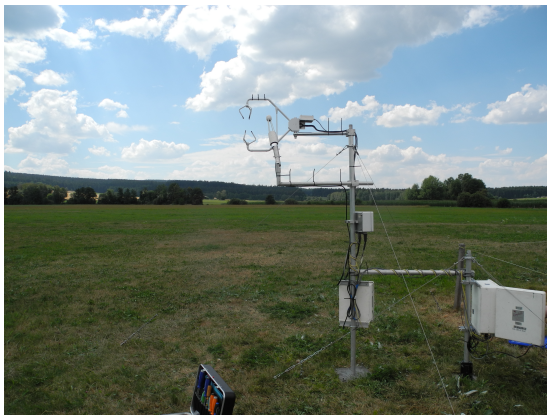


Figure A.2.: Scatter plot between measured long-wave upwelling radiation (I_{\uparrow}) (available data) and calculated I_{\uparrow} in the time period 01.06.2010 - 01.09.2010.

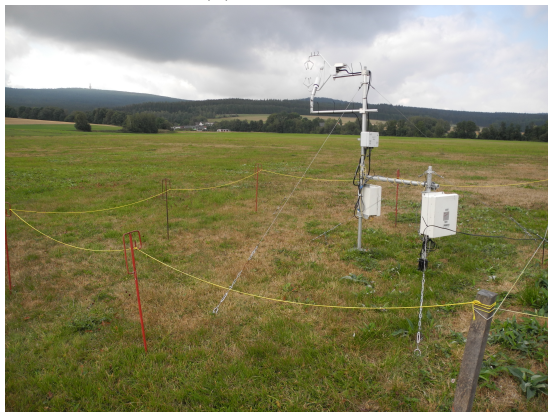
A.3. Photo series of the site



(a) 30.07.2018



(b) 18.08.2018



(c) 28.08.2018



(d) 28.08.2018, brown grass

A.3. Photo series of the site



(e) 28.08.2018, green grass



(f) 18.09.2018



(g) 04.10.2018



(h) 17.10.2018

Figure A.3.: Series of photos of the measurement site taken during maintenance work.

Declaration of Authorship

I hereby declare that the thesis titled “Carbon and energy exchange at a submontane grassland site in an extremely dry year” is my own unaided work. All direct or indirect sources used are acknowledged as references. This paper was not previously presented to another examination board and has not been published.

Hiermit erkläre ich, dass ich die vorgelegte Arbeit „Carbon and energy exchange at a submontane grassland site in an extremely dry year“ eigenständig verfasst und keine anderen als die im Literaturverzeichnis angegebenen Quellen und Hilfsmittel benutzt habe. Weiter wurde diese Arbeit bisher nicht veröffentlicht oder zur Erlangung eines akademischen Grades eingereicht.

Bayreuth,

Valentin Heinzelmann
